A linear analysis of the hybrid Kelvin-Helmholtz/Rayleigh-Taylor instability in an electrostatic magnetosphere-ionosphere coupling system

T. Yamamoto[1]

Received 2 October 2007; revised 5 December 2007; accepted 14 January 2008; published 10 June 2008.

[1] A linear analysis of the hybrid Kelvin-Helmholtz/Rayleigh-Taylor (KH/RT) instability in the magnetosphere-ionosphere coupling system is presented. In the magnetosphere plasma particles can move by the electric ($\mathbf{E} \times \mathbf{B}$) drift, magnetic drift (gradient B drift plus curvature drift), and inertia drift. Field-aligned currents are generated primarily from divergence of the magnetic drift flux. They are closed via Pedersen currents in the ionosphere. As a simple model, there is a surface of discontinuity both in the azimuthal flow and the particle energy density, which extends longitudinally as projected to the ionospheric plane. The gradient of the energy density is directed inward or outward so that the plasma is RT unstable or stable, respectively. The present analysis shows that only a velocity shear cannot drive the system KH unstable when the growth rate, γ_{KH}, of the KH instability without Pedersen coupling is less than the inertial relaxation rate, ν, and that the presence of an energy density gradient allows a hybrid wave to grow even when $\gamma_{KH} < \nu$. The wave growth is due to the active charge separation driving originally the RT instability. The picture of auroral deformations now changes drastically. The traditional picture is such that if the Pedersen coupling is properly taken into account, KH waves of long wavelengths ($\gtrsim$100 km at the ionospheric height) are found evanescent in the main body of the auroral oval. A new one is such that wavy structures therein can develop, only in the KH/RT hybrid mode, at the places where the particle energy density has an inward gradient. Similarly, the stability of the inner boundary of the low-latitude boundary layer is controlled by the RT stability conditions more influentially than the KH conditions.

Citation: Yamamoto, T. (2008), A linear analysis of the hybrid Kelvin-Helmholtz/Rayleigh-Taylor instability in an electrostatic magnetosphere-ionosphere coupling system, *J. Geophys. Res.*, *113*, A06206, doi:10.1029/2007JA012850.

1. Introduction

[2] The Kelvin-Helmholtz (KH) instability has been widely studied for understanding a variety of phenomena in magnetospheric physics such as the ULF pulsations in the Pc3 to Pc5 ranges [e.g., *Walker*, 1981], auroral deformations [e.g., *Hallinan and Davis*, 1970; *Miura and Sato*, 1978; *Wagner et al.*, 1983; *Murphree et al.*, 1994; *Yamamoto et al.*, 1994], and the momentum or mass transport of the solar wind plasma across the low-latitude boundary layer (LLBL) [e.g., *Axford and Hines*, 1961; *Sckopke et al.*, 1981; *Miura*, 1995; *Fairfield et al.*, 2000; *Matsumoto and Hoshino*, 2006]. An important fact influencing the KH instability in the magnetosphere is that the field lines are connected to the conductive ionosphere [e.g., *Lotko et al.*, 1987; *Lotko and Shen*, 1991; *Lysak et al.*, 1995]. *Keskinen et al.* [1988] performed the first numerical simulation of the electrostatic KH instability with ionospheric Pedersen conductivity coupling. *Wei and Lee* [1993] conducted a numerical simulation for the development of KH-produced plasma vortices in a system of the LLBL-ionosphere electrostatic coupling. *Miura and Kan* [1992] showed the stabilizing effect of the ionospheric line-tying on the magnetohydrodynamic KH instability through a three-dimensional linear analysis.

[3] A number of authors [e.g., *Wolf*, 1983; *Southwood and Kivelson*, 1987, 1989] have believed that the low-energy (0.1–10 keV) particle population in the plasma sheet is basically stable to the Rayleigh-Taylor (RT) instability, while the RT instability at the plasmapause has been discussed by, for example, *Richmond* [1973] and that in the Van Allen belt by, for example, *Chang et al.* [1965]. On the contrary, the numerical simulation by *Yamamoto et al.* [1997a] showed that the auroral omega bands may be the manifestation of RT waves growing in the plasma sheet. This result suggests that the plasma sheet assumes an RT-unstable configuration, at least in the recovery phase of a substorm during which omega bands are frequently observed. According to the simulation for the generations of the region 0, region 1 and region 2 field-aligned currents (FACs) [*Yamamoto and Inoue*, 2004, hereinafter referred to

[1]Department of Earth and Planetary Science, University of Tokyo, Tokyo, Japan.

0148-0227/08/2007JA012850

as YI04], the region 1 FACs [e.g., *Iijima and Potemra*, 1978] are produced around the interface between nonadiabatic and adiabatic plasmas where the particle energy density has an inward (equatorward as mapped to the ionosphere) gradient. (This gradient essentially comes from the nonadiabatic acceleration of particles in the tail current sheet.) In such a place the plasma is potentially unstable to the RT instability. It is interesting to note here the earlier observational inference by *Goertz and Baumjohann* [1991]: the plasma sheet contains a mixture of high-entropy (i.e., low-density and high-temperature) ''bubbles'' and low-entropy ''blobs''. (For explanation of bubbles and blobs, see also *Pontius and Wolf* [1990].) This signature may be interpreted as a consequence of frequent occurrence of the RT instability in the tail plasma sheet.

[4] Considerable attention has been paid to the coupling of the KH instability and the RT instability in the terrestrial magnetosphere/ionosphere. For example, *Farrugia et al.* [1998] theoretically studied the hybrid KH/RT instability at the dayside magnetopause, in a situation that it is in accelerated motion, being subject to an effective gravitational field. *Hysell and Kudeki* [2004] discussed a possibility that the KH instability competes with the collisional RT instability in the equatorial *F* region ionosphere under some conditions. *Matsumoto and Hoshino* [2006] suggested that the nonlinear coupling of the KH and RT instabilities play an important role, through turbulent mixing of plasmas, in the transport mechanism of the solar wind plasma into the Earth magnetosphere, while they did not study the linear coupling. In general, the charge separation perpendicular to the field lines that drives the RT instability in the magnetosphere is short-circuited by the large electron conductivity in the parallel direction, producing field-aligned currents which close in the ionosphere. So far, however, little attention has been paid to such discharging effect on the hybrid KH/RT instability, at least, in magnetospheric physics.

[5] The present paper is a first theoretical study on the hybrid KH/RT instability in the magnetosphere-ionosphere (M-I) coupling system. The growth of a hybrid wave will be shown to be determined as a balance of the four agents: velocity shear, energy density gradient, inertial effect, and ionospheric conductivity. Particular emphases are to be laid on the hybrid wave growth in a situation that a KH wave is evanescent and on the hybrid wave stability in a situation that a KH wave grows.

2. Basic Equations for M-I Coupling

[6] The present analysis is electrostatic so that the effect of the Alfvén wave transmission in the magnetosphere is neglected. (For this approximation, the wave growth time, γ^{-1}, is required to be longer than the transit time of an Alfvén wave between the ionosphere and the equator; roughly, γ^{-1} should be greater than a few minutes.) The drift approximation is used for the perpendicular motions of particles for slow and large-scale phenomena of temporal and spatial scales much greater than the ion cyclotron period and radius, respectively. For the analysis of an electrostatic instability, the conservation of space charge in the M-I coupling need to be described mathematically.

[7] The flux tube content, N^j, is defined as the number of particles of species j (***p***roton or ***e***lectron) in a flux tube with unit (ionospheric) cross section:

$$N^j \equiv \int_{s_i}^{s_e} n^j(s)\frac{B_i}{B(s)}ds, \tag{1}$$

where $n^j(s)$ is the number density of species j, s is the field-aligned distance, s_e and s_i are the distances to the equator and the ionospheric height, respectively; $B(s)$ and B_i are the magnetic field intensities at distances s and s_i, respectively. (In the present analysis a hydrogen plasma is assumed unless otherwise stated, and the field lines are assumed to be closed.) Provided that the velocity distribution of particles is isotropic, $n^j(s)$ is constant along a field line so that equation (1) is reduced to $N^j = n^j B_i R_B$, where R_B is the flux tube volume defined as

$$R_B \equiv \int_{s_i}^{s_e} \frac{1}{B(s)}ds. \tag{2}$$

The flux tube energy content, $\mathcal{E}$, of protons is defined as the integral over the flux tube volume:

$$\mathcal{E} \equiv \int_{s_i}^{s_e} wn^p \frac{B_i}{B(s)}ds = wN^p, \tag{3}$$

where w is the proton kinetic energy averaged in velocity space and it is independent of s because of isotropy of the velocity distribution.

[8] The flux tube content N^j must satisfy the particle conservation law in the ionospheric plane:

$$\frac{\partial}{\partial t}N^j + \mathrm{div}\,\boldsymbol{\Gamma}^j = Q^j - L^j, \tag{4}$$

where div is operated in the ionospheric plane which is assumed to be perpendicular to the ambient magnetic field $\boldsymbol{B}_i$; the particle influx Q^j and outflux L^j represent supply from and precipitation into the ionosphere, respectively. The lateral particle flux $\boldsymbol{\Gamma}^j$ is defined as

$$\begin{aligned}\boldsymbol{\Gamma}^j &= \boldsymbol{\Gamma}_E^j + \boldsymbol{\Gamma}_m^j + \boldsymbol{\Gamma}_{in}^j + \boldsymbol{\Gamma}_d^j \\ &\equiv \int_{s_i}^{s_e} \sum \left(\boldsymbol{V}_E(s) + \boldsymbol{V}_m^j(s) + \boldsymbol{V}_{in}^j(s) + \boldsymbol{V}_d^j(s)\right)\frac{B_i}{B(s)}ds,\end{aligned} \tag{5}$$

where $\sum$ denotes the summation over all the particles of species j in unit volume; $\boldsymbol{V}_E(s)$, $\boldsymbol{V}_m^j(s)$, $\boldsymbol{V}_{in}^j(s)$, and $\boldsymbol{V}_d^j(s)$ are the ionospheric projections of the electric drift, magnetic drift (gradient B drift plus curvature drift), inertia drift, and cross-field diffusion velocities (see Appendix C of YI04) of a particle of species j, respectively. The fluxes $\boldsymbol{\Gamma}_E^j$, $\boldsymbol{\Gamma}_{in}^j$, $\boldsymbol{\Gamma}_m^j$, and $\boldsymbol{\Gamma}_d^j$ are then termed the electric drift, magnetic drift, inertia drift, and cross-field diffusion fluxes, respectively.

[9] Assuming the equipotential field lines, the electric drift velocity $\boldsymbol{V}_E(s)$ at any distance s is found to be identical to $\boldsymbol{V}_E(s_i)$, i.e., the electric drift velocity in the ionospheric plane. (Hereafter $\boldsymbol{V}_E(s_i)$ is simply denoted by $\boldsymbol{V}_E$.) The flux of $\boldsymbol{\Gamma}_E^j + \boldsymbol{\Gamma}_m^j + \boldsymbol{\Gamma}_{in}^j$ in equation (5) is then written as

$$\boldsymbol{\Gamma}_E^j + \boldsymbol{\Gamma}_m^j + \boldsymbol{\Gamma}_{in}^j = N^j\left(\boldsymbol{V}_E + \boldsymbol{V}_m^j + \boldsymbol{V}_{in}^j\right), \tag{6}$$

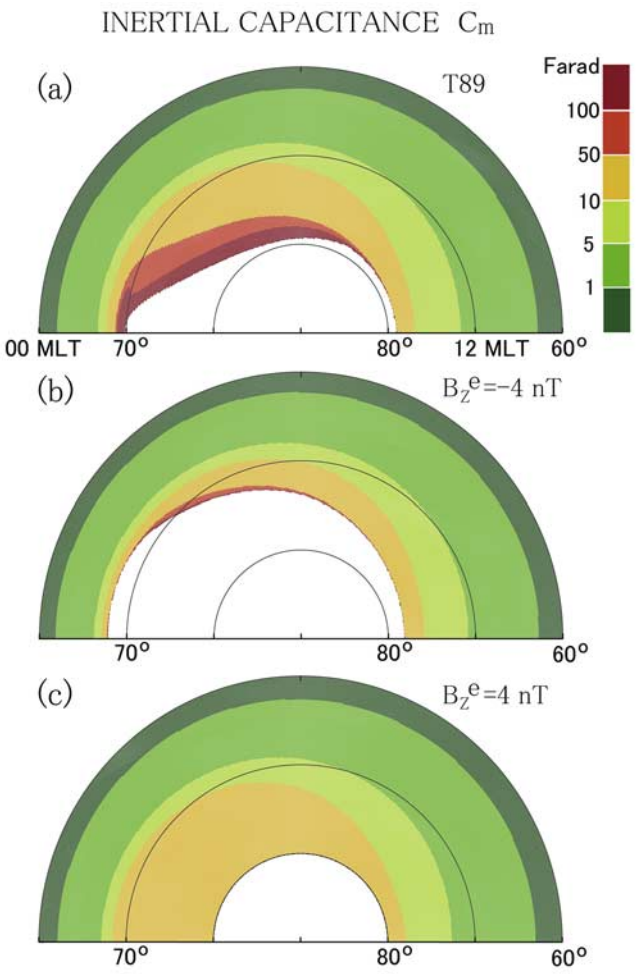

Figure 1. Two-dimensional plots of the inertial capacitance C_m in the ionospheric plane, where the noon/midnight meridian and the 60°, 70°, and 80° magnetic latitude lines are indicated. It is calculated in the magnetically closed region at latitudes less than 80°, using the $Kp = 0$ version of the Tsyganenko model [*Tsyganenko*, 1989] with an additional constant Z-component (B_Z^e) of −4 nT, in (b), or 4 nT, in (c). (Such addition is to include the effect of the IMF B_Z penetration into the magnetosphere; a nontilted dipole is used as the field from the Earth's interior.) For representing C_m for the plasma sheet, it is assumed that the number density n changes spatially under the conditions that the flux tube content nB_iR_B is constant and n is 1 cm^{-3} at places where the flux tube volume is equal to the reference flux tube volume defined in section 4, i.e., $R_B = R_{B,0}$.

where $\boldsymbol{V}_m^j$ and $\boldsymbol{V}_{in}^j$ are the averaged magnetic drift and inertia drift velocities which are defined as

$$\boldsymbol{V}_m^j = \frac{1}{N^j}\int_{s_i}^{s_e} \sum \boldsymbol{V}_m^j(s)\frac{B_i}{B(s)}ds \tag{7}$$

and

$$\boldsymbol{V}_{in}^j = \frac{1}{N^j}\int_{s_i}^{s_e} \sum \boldsymbol{V}_{in}^j(s)\frac{B_i}{B(s)}ds, \tag{8}$$

respectively. The average magnetic drift velocity per unit energy, $\boldsymbol{\nu}_m$, is defined as

$$\boldsymbol{\nu}_m = \frac{1}{R_B}\int_{s_i}^{s_e} \frac{1}{wn^p} \sum \boldsymbol{V}_m^p(s)\frac{1}{B(s)}ds = \frac{\boldsymbol{V}_m^p}{w}, \tag{9}$$

and it is shown to be expressed as [*Vasyliunas*, 1970; *Yamamoto et al.*, 1996]

$$\boldsymbol{\nu}_m = -\frac{2}{3e}\frac{1}{R_B B_i}\boldsymbol{b}_i \times \nabla R_B, \tag{10}$$

where e (>0) is the electronic charge and $\boldsymbol{b}_i$ is the unit vector in the direction of $\boldsymbol{B}_i$. Neglecting $\nabla_\perp B_i$ as well as rot$\boldsymbol{B}_i$ (because the ionospheric field $\boldsymbol{B}_i$ is well approximated by the dipole field) leads to the conditions of

$$\mathrm{div}\,\boldsymbol{V}_E = 0 \quad \text{and} \quad \mathrm{div}\,\boldsymbol{\nu}_m = 0. \tag{11}$$

The validity of these conditions is shown in Appendix A, item 1.

[10] It is assumed that the protons obey the adiabatic equation of state, specifically $wR_B^{2/3}$ is conserved along the trajectory of a "proton fluid" which moves in the ionospheric plane with the total velocity, $\boldsymbol{V}_t$, of $\boldsymbol{V}_E + \boldsymbol{V}_m^p$ [*Wolf*, 1983]:

$$\frac{d}{dt}\left(wR_B^{2/3}\right) \equiv \left(\frac{\partial}{\partial t} + \boldsymbol{V}_t \cdot \nabla\right)\left(wR_B^{2/3}\right) = 0. \tag{12}$$

Noting that $\boldsymbol{\nu}_m$ is perpendicular to ∇R_B (see equation (10)), $\boldsymbol{\nu}_m \cdot \nabla w$ vanishes for the case of $w \propto R_B^{-2/3}$. In this case, from conditions of (11), the conservation of protons in a flux tube, equation (4), is reduced to

$$dN^p/dt = -\mathrm{div}\,\boldsymbol{\Gamma}_d^p, \tag{13}$$

where both Q^p and L^p for protons are assumed negligible (see Appendix B of YI04) and $\boldsymbol{\Gamma}_{in}^p$ is neglected. (For conditions for this assumption, see Appendix A, item2.) Using the relation of $\mathcal{E} = wN^p$, combination of equations (12) and (13) yields

$$\frac{d}{dt}\left(\mathcal{E}R_B^{2/3}\right) = -wR_B^{2/3}\mathrm{div}\,\boldsymbol{\Gamma}_d^p. \tag{14}$$

Because $\boldsymbol{\Gamma}_d^p$ is expressed as $\boldsymbol{\Gamma}_d^p = -(D/w)\nabla\mathcal{E}$ [YI04], where D is the diffusion rate for the ionospheric projections of protons, averaged over the flux tube volume, equation (14) may be written as

$$d\mathcal{E}^*/dt = D\nabla^2\mathcal{E}^*, \tag{15}$$

where $\mathcal{E}^* \equiv \mathcal{E}R_B^{2/3}$ is a conserved quantity in the case of vanishing divergence of $\boldsymbol{\Gamma}_d^p$ and the spatial variations of D/w and $R_B^{2/3}$ are ignored for retaining only lowest-order effects of diffusion. (For some details, see Appendix A, item 3.)

[11] An approximate expression for the inertia (polarization) drift flux of protons may be given by

$$\boldsymbol{\Gamma}_{in}^p = (C_m/e)d\boldsymbol{E}/dt, \tag{16}$$

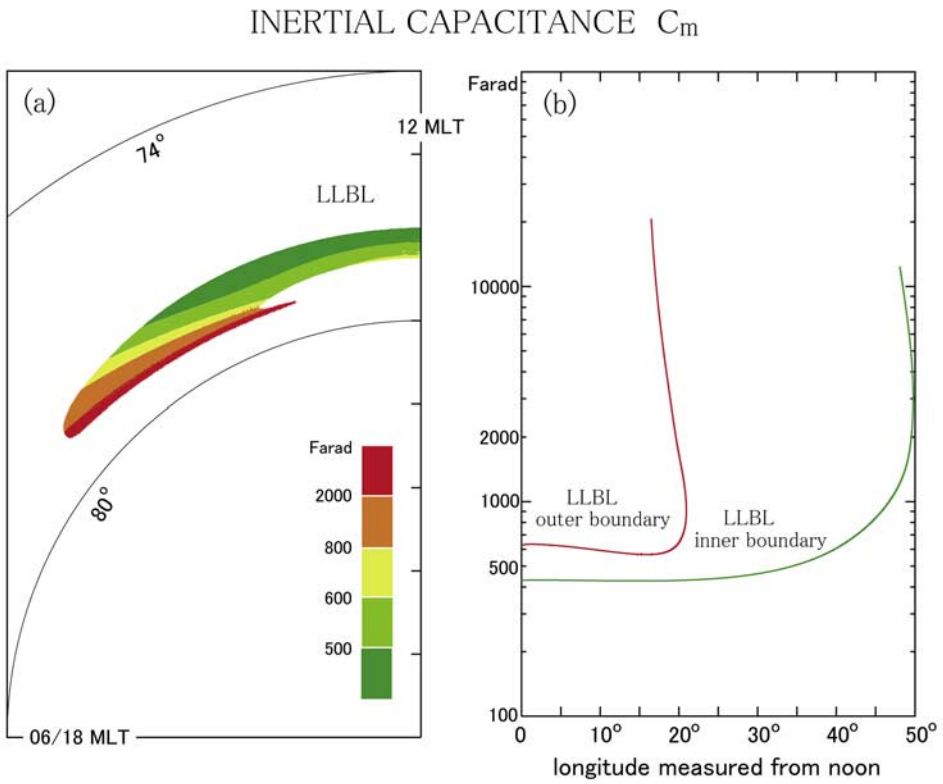

Figure 2. (a) Two-dimensional plot of C_m in the low-latitude boundary layer (LLBL) as modeled by *Kaufmann et al.* [1993] and *Yamamoto and Ozaki* [2005]. The evaluation of C_m is based on the $Kp = 0$ version of the 1989 Tsyganenko model. It is assumed that n changes spatially under the conditions that nB_iR_B is constant and n is 1 cm^{-3} at $X = 0$ on the outer boundary of the closed LLBL, where $R_B = 33.7R_{B,0}$. (This point is mapped to an ionospheric position of 78.9° in latitude and 13.3 in MLT.) (b) Profiles of C_m along the inner and outer boundaries of the closed LLBL, which are plotted against the longitude (in degree) measured from the noon meridian. Extremely high values (>10^3 F) of C_m come from great volumes of the flux tubes extending far away from the Earth. The values in this figure are for the flux tubes loaded "fully" with LLBL particles, i.e., having the constant content of nB_iR_B. Actual values of C_m around the inner boundary will be given roughly by halving the values in the figure and neglecting smaller contributions from the plasma sheet (in Figures 1a–1c). Thus the LLBL inner boundary has values of C_m greater than ∼200 F.

where $\boldsymbol{E}$ is the ionospheric electric field perpendicular to the magnetic field. The inertial capacitance, C_m [e.g., *Keskinen et al.*, 1988], is defined as

$$C_m \equiv \int_{s_i}^{s_e} \frac{Mn^p(s)}{B(s)^2} ds, \tag{17}$$

where M is the proton mass. For the conditions required for that approximation, see Appendix A of *Yamamoto et al.* [1996], while the expression for $\boldsymbol{\Gamma}^p_{in}$, equation (16), turns out to be relevant for studying how the "classical" KH instability is modified by the RT instability. (Examples of the distributions of C_m in the magnetosphere are shown in Figures 1 and 2.)

[12] The flux tube volume below a low-altitude region of field-aligned electric fields accelerating electrons [e.g., *Mozer and Hull*, 2001] is only a small fraction of the total flux tube volume. For the majority of plasma particles in the magnetosphere, the temperature of electrons can then be assumed to be even lower than the ion temperature. In the present analysis, electrons are treated as cold particles so that their magnetic drift flux, $\boldsymbol{\Gamma}^e_m$, is neglected, and the electron inertia drift is also neglected.

[13] The total electron flux of $e(L^e - Q^e)$ is considered to be an FAC density, $J_\parallel$, at the ionospheric height. A positive value of $J_\parallel$ is for an upward (i.e., flowing away from the Earth) FAC. Then, subtracting conservation equation (4) for the proton flux tube content (N^p) from that for the electron one, the charge neutrality condition of $N^p \simeq N^e$ yields

$$J_\parallel = e(L^e - Q^e) = e\,\mathrm{div}\left(\boldsymbol{\Gamma}^p_m + \boldsymbol{\Gamma}^p_{in} + \boldsymbol{\Gamma}^p_d\right), \tag{18}$$

where $\boldsymbol{\Gamma}^e_m$ and $\boldsymbol{\Gamma}^e_{in}$ are neglected as assumed above, and $\boldsymbol{\Gamma}^e_d$ can be neglected as discussed by *Yamamoto et al.* [1997b]; $J_{\parallel m} \equiv e$ div $\boldsymbol{\Gamma}^p_m$ and $J_{\parallel d} \equiv e$ div $\boldsymbol{\Gamma}^p_d$ are current densities of the magnetic-drift-induced and diffusion-induced FACs, respectively. While the diffusion-induced FACs are thought to be responsible for the generation of the region 0 FACs [YI04] and the formation of discrete auroras [*Yamamoto et al.*, 1999], they may be ignored for simple discussion on the

KH and RT instabilities. Using $\boldsymbol{\Gamma}_m^p = \mathcal{E}\boldsymbol{\nu}_m$, div $\boldsymbol{\nu}_m = 0$ and $\boldsymbol{\nu}_m \cdot \nabla R_B = 0$, the current density $J_{\parallel m}$ can be written as

$$J_{\parallel m} = e\,\boldsymbol{\nu}_m \cdot \nabla\mathcal{E} = e\,R_B^{-2/3}\boldsymbol{\nu}_m \cdot \nabla\mathcal{E}^*. \tag{19}$$

[14] The current continuity in the uniform ionosphere is expressed as

$$\Sigma_P\nabla^2\phi = -\Sigma_P \mathrm{div}\,\boldsymbol{E} = J_\parallel, \tag{20}$$

where ϕ is the electrostatic potential and Σ_P is the height-integrated Pedersen conductivity. Note that divergence of the Hall current is negligible for uniform height-integrated conductivities. Finally, combination of equations (16) and (18)–(20) yields

$$\mathrm{div}\left(C_m\frac{d}{dt}\nabla\phi\right) = -\Sigma_P\nabla^2\phi + e\,R_B^{-2/3}\boldsymbol{\nu}_m \cdot \nabla\mathcal{E}^*. \tag{21}$$

Using $\boldsymbol{V}_E = \boldsymbol{b}_i \times \nabla\phi/B_i$ and neglecting the spatial variations of C_m and $\boldsymbol{V}_m^p$, the above equation is rewritten as

$$C_m\frac{d}{dt}\nabla^2\phi = -\Sigma_P\nabla^2\phi + e\,R_B^{-2/3}\boldsymbol{\nu}_m \cdot \nabla\mathcal{E}^*. \tag{22}$$

The C_m and $\boldsymbol{V}_m^p$ variations may not be neglected in regions relatively near the open/closed boundary. Retaining such inhomogeneity, however, would bring about some difficulty in elucidating the coupling between the KH and RT instabilities both in standard form.

3. Linearized Equations

[15] Equation (22) is to be solved, under the condition of (15), for a small amplitude perturbation in potential, $\delta\phi$:

$$\phi = \phi_0 + \delta\phi = \phi_0(x) + \delta\phi(x)\exp i\big(k_y y - \omega t\big), \tag{23}$$

where ϕ_0 is the unperturbed part of ϕ; ω is the wave frequency and k_y (>0) is the azimuthal wave number ($2\pi/\lambda$). Here the (local) Cartesian coordinates x, y and z are taken such that the directions of positive x and y are poleward and westward in the ionospheric plane, respectively; the directions of $\boldsymbol{B}_i$ and $\boldsymbol{\nu}_m$ are assumed to be in the negative z-direction and positive y-direction, respectively. When ϕ_0 is assumed uniform azimuthally, the unperturbed electric drift velocity has only a y-component of $V_{E,0}(x)$. In harmony with $\phi_0 + \delta\phi$ in equation (23), the "flux tube energy content" $\mathcal{E}^*$ is decomposed as

$$\mathcal{E}^* = \mathcal{E}_0^* + \delta\mathcal{E}^* = \mathcal{E}_0^*(x) + \delta\mathcal{E}^*(x)\exp i\big(k_y y - \omega t\big). \tag{24}$$

[16] The linearized form of equation (15) is obtained by substituting equations (23) and (24) into it:

$$\begin{aligned} &i\big(\omega - k_y V_t(x)\big)\delta\mathcal{E}^*(x) - i\big(k_y/B_i\big)\delta\phi(x)\mathcal{E}_0^{*\prime}(x) \\ &\quad = D\Big(k_y^2\delta\mathcal{E}^*(x) - \delta\mathcal{E}^{*\prime\prime}(x)\Big), \end{aligned} \tag{25}$$

where $V_t(x)$ is the unperturbed westward drift velocity, i.e., $V_t(x) = V_{E,0}(x) + |\boldsymbol{V}_m^p|$; $d\mathcal{E}^*{}_0(x)/dx$ is denoted by $\mathcal{E}_0^{*\prime}(x)$. (The unperturbed part of equation (15) is the diffusion equation of $\partial\mathcal{E}_0^*/\partial t = D\nabla^2\mathcal{E}_0^*$.) Linearizing equation (22) results in

$$\begin{aligned} &\big(\omega - k_y V_t(x) + i\nu\big)\Big(-k_y^2\delta\phi(x) + \delta\phi''(x)\Big) + k_y V_{E,0}{}''(x)\delta\phi(x) \\ &\quad = -k_y e\,\frac{R_B^{-2/3}}{C_m}\nu_m\delta\mathcal{E}^*(x), \end{aligned} \tag{26}$$

where $\nu_m = |\boldsymbol{\nu}_m|$ and ν is the inertial relaxation rate Σ_P/C_m [*Lotko et al.*, 1987; *Keskinen et al.*, 1988].

4. Coupling Between KH and RT Instabilities

[17] To study the coupling between the KH and RT instabilities both in standard form, the diffusion term is dropped in equation (25). (The diffusion effect on the RT instability is studied in Appendix B.) Eliminating $\delta\mathcal{E}_0^*(x)$ from equations (25) and (26), the mode equation for the hybrid KH/RT instability is given by

$$\begin{aligned} &\big(\omega - k_y V_t(x) + i\nu\big)\Big(-k_y^2\delta\phi(x) + \delta\phi''(x)\Big) + k_y V_{E,0}{}''(x)\delta\phi(x) \\ &\quad = \nu\gamma_m(x)\,\frac{k_y^2\delta\phi(x)}{\omega - k_y V_t(x)}, \end{aligned} \tag{27}$$

where $\gamma_m(x)$ is defined as $\gamma_m(x) = -(e\nu_m/B_i\Sigma_P R_B^{2/3})\mathcal{E}_0^{*\prime}(x)$. When $\gamma_m(x) \equiv 0$, $\boldsymbol{V}_m^p = 0$ and $\Sigma_P = 0$ (hence $\nu = 0$), the above equation is reduced to

$$\delta\phi''(x) + \left(-k_y^2 + \frac{k_y V_{E,0}{}''(x)}{\omega - k_y V_{E,0}}\right)\delta\phi(x) = 0, \tag{28}$$

which gives the standard dispersion relation for the transverse KH instability [e.g., *Michalke*, 1964]. Following the conventional reduction [e.g., *Keskinen et al.*, 1988], equation (27) is rewritten as

$$\begin{aligned} \frac{d}{dx}\left(A(x)\frac{d\Phi(x)}{dx}\right) &= k_y^2 A(x) \\ &\cdot\left\{1 + \frac{\nu\gamma_m(x)}{\big(\omega - k_y V_t(x)\big)\big(\omega - k_y V_t(x) + i\nu\big)}\right\}\Phi(x), \end{aligned} \tag{29}$$

where $A(x) = (\omega - k_y V_t(x) + i\nu)^2$ and $\Phi(x) = \delta\phi(x)/(\omega - k_y V_t(x) + i\nu)$. When $\Sigma_P = 0$, hence $\nu = 0$ but $\nu\gamma_m(x)$ (independent of Σ_P) is retained, this equation itself is essentially identical to that describing the joint KH and RT instabilities at the magnetopause under the conditions of $\boldsymbol{k} \cdot \boldsymbol{B} = 0$ and $\partial\rho/\partial\overline{y} = 0$ in H [see *Farrugia et al.*, 1998]. Besides the equivalent gravity force ($g \leftrightarrow ew\nu_m N/C_m B_i$), the main difference is only the appearance of the Doppler-shifted frequency $\omega - k_y V_t$ in the gravitational term here instead of $\omega - k_y V_{E,0}$. The former type of Doppler shift necessarily arises when plasma particles move by the magnetic drift, which is the cause of the "gravity force".

[18] A velocity shear may appear in the region where the energy density has a significant gradient, primarily, in latitude, as will be the case with, for example, the generation of the region 1 FACs in the plasma sheet [YI04] and in the low-latitude boundary layer [*Yang et al.*, 1994; *Yamamoto et*

al., 2002]. The FAC generation is possible in a situation that the energy density has a gradient in the direction of the average magnetic drift while the azimuthal gradient is even smaller in magnitude than the latitudinal one. For a simple solution to equation (29), consider a two-dimensional system with a sharp boundary at $x = 0$: The x dependence of $V_{E,0}(x)$ is taken as

$$V_{E,0}(x) = V_{E,0}(0) + \lim_{L_\varepsilon \to +0} \Delta_V \tanh(x/L_\varepsilon). \tag{30}$$

The profile of $\mathcal{E}^*_0(x)$ has a jump of $\Delta_\mathcal{E}$ at $x = 0$ so that

$$\frac{d\mathcal{E}^*_0(x)}{dx} = -\Delta_\mathcal{E}\delta(x), \tag{31}$$

where $\delta(x)$ is the Dirac delta function. In this system $\gamma_m(x)$ is written as

$$\gamma_m(x) = u_m\delta(x), \tag{32}$$

where $u_m \equiv (e\nu_m/B_i\Sigma_P R_B^{2/3})\Delta_\mathcal{E}$. In either region of $x > 0$ or $x < 0$, the solution to equation (29) is then expressed as $\Phi(x) = a_+ \exp(-k_y x)$ or $\Phi(x) = a_- \exp(k_y x)$, respectively. The step function profile in $V_{E,0}(x)$ or $\mathcal{E}^*_0(x)$ may limit the analysis to the case of long wavelength as $k_y L/2 = \pi L/\lambda \ll 1$ [*Keskinen et al.*, 1988; *Huba*, 1996a], where L stands for the actual scale length for $dV_{E,0}(x)/dx$ and $d\mathcal{E}^*_0(x)/dx$. The applicability of the long wavelength approximation will be discussed later.

[19] The matching conditions at $x = 0$ are obtained by the following integrations of equation (29):

$$\left[A(x)\frac{d\Phi(x)}{dx}\right]_{-\varepsilon}^{\varepsilon} = \int_{-\varepsilon}^{\varepsilon} dx k_y^2 A(x) \cdot \left\{1 + \frac{\nu\gamma_m(x)}{(\omega - k_y V_t(x))(\omega - k_y V_t(x) + i\nu)}\right\}\Phi(x) \tag{33}$$

and

$$[\Phi(x)]_{-\varepsilon}^{\varepsilon} = \int_{-\varepsilon}^{\varepsilon} dx' \frac{1}{A(x')} \int_{-\infty}^{x'} dx k_y^2 A(x) \cdot \left\{1 + \frac{\nu\gamma_m(x)}{(\omega - k_y V_t(x))(\omega - k_y V_t(x) + i\nu)}\right\}\Phi(x). \tag{34}$$

In the limit of $\varepsilon \to 0$, these equations are reduced to

$$-k_y A(+0)a_+ - k_y A(-0)a_- = k_y^2 A(0) \cdot \left\{\frac{\nu u_m}{(\omega - k_y V_t(0))(\omega - k_y V_t(0) + i\nu)}\right\}\Phi(0) \tag{35}$$

and

$$a_+ - a_- = 0. \tag{36}$$

The dispersion relation is then given by

$$(\omega - k_y V_t(+0) + i\nu)^2 + (\omega - k_y V_t(-0) + i\nu)^2 = -\frac{k_y\nu u_m(\omega - k_y V_t(0) + i\nu)}{\omega - k_y V_t(0)}. \tag{37}$$

Let the frequency ω be expressed as

$$\omega = k_y V_t(0) + i\gamma, \tag{38}$$

where the phase velocity is assumed to be $V_t(0)$ and γ is the growth rate with a positive value for growth. Let the growth rates associated with the KH and RT instabilities, γ_{KH} and γ_{RT}, be defined as

$$\gamma_{KH} = k_y\Delta_V \quad \text{and} \quad \gamma_{RT} = k_y u_m/2 = \left(e\nu_m/B_i\Sigma_P R_B^{2/3}\right)k_y\Delta_\mathcal{E}/2, \tag{39}$$

respectively. (If $k_y < 0$ is assumed, $\gamma_{RT} \equiv -k_y u_m/2 = |k_y|u_m/2$.) Exactly, the former is the growth rate of the KH instability without Pedersen coupling, in other words the KH growth rate in the magnetosphere connected with an insulated ionosphere, while the latter is the RT growth rate in the limit of $C_m \to 0$, in the M-I coupling system. Variables being normalized by ν, denoted by ˜ (for example, $\tilde\gamma = \gamma/\nu$), equation (37) is written as

$$-(1 + \tilde\gamma)^2 + \tilde\gamma_{KH}^2 + \tilde\gamma_{RT}\frac{1 + \tilde\gamma}{\tilde\gamma} = 0. \tag{40}$$

Unless $\tilde\gamma = 0$, the above equation is equivalent to

$$F(\tilde\gamma) \equiv \tilde\gamma^3 + 2\tilde\gamma^2 + (1 - \tilde\gamma_{KH}^2 - \tilde\gamma_{RT})\tilde\gamma - \tilde\gamma_{RT} = 0. \tag{41}$$

Except for the case of $\tilde\gamma_{RT} = 0$, the marginal stability of $\tilde\gamma = 0$ cannot be treated by the present theory, because the denominator of the third term in equation (40) vanishes.

4.1. Analytic Solution

[20] If $\tilde\gamma_{RT} > 0$, the function $F(\tilde\gamma)$ defined in equation (41) has the following characteristics: $F(0) < 0$ and the equation of $dF(\tilde\gamma)/d\tilde\gamma = 0$ has at least one negative solution. Therefore the equation of $F(\tilde\gamma) = 0$ has only one positive solution when $\tilde\gamma_{RT} > 0$.

[21] For the case of $\tilde\gamma_{RT} = 0$, the solution to equation (40) without the third term, for a growing wave, is

$$\tilde\gamma = \tilde\gamma_{KH} - 1 \quad (\text{i.e.}, \gamma = \gamma_{KH} - \nu) \quad \text{for} \quad \tilde\gamma_{KH} > 1. \tag{42}$$

Needless to say, this solution can also be obtained from equation (41), setting $\tilde\gamma_{RT}$ at 0, but that equation has a spurious solution of $\tilde\gamma = 0$ as noted above. As already addressed, the growth rate in the limit of $\Sigma_P \to 0$ is given by γ_{KH}. Moreover, equation (42) indicates that the growth rate γ of the KH instability can be significantly decreased by the effect of the M-I coupling, as predicted by *Keskinen et al.* [1988]. (A comparison of their model with the present one in the Pedersen conductivity coupling of the KH instability is further discussed in Appendix C.) This effect is promoted

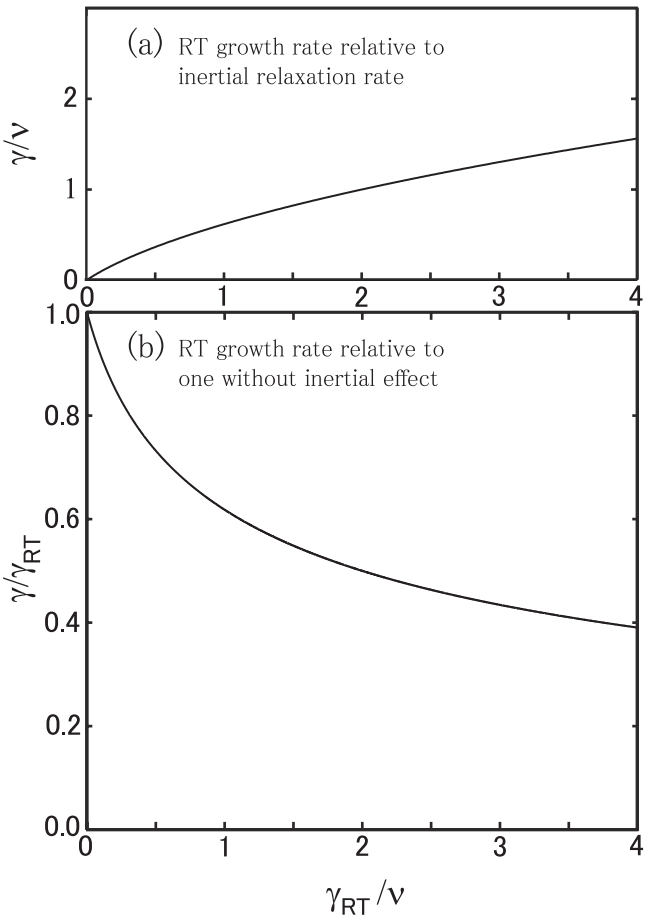

Figure 3. Growth rate of the fastest growing mode, a solution to equation (41) for the case of $\tilde{\gamma}_{KH} = 0$: (a) $\tilde{\gamma} = \gamma/\nu$ and (b) γ/γ_{RT}, which are given by equation (43), are plotted against $\tilde{\gamma}_{RT}$ (>0).

by higher Pedersen conductivity and smaller inertial capacitance.

[22] Equation (42) indicates the existence of a critical condition for the onset of the KH instability in the M-I coupling system: γ_{KH} is required to exceed ν. Such a condition is quite important for understanding the auroral phenomena in the magnetosphere-ionosphere system. Without it, the system should be full of KH waves, because a velocity shear, i.e., space charge exists practically everywhere.

[23] For the case of $\tilde{\gamma}_{KH} = 0$, equation (41) has a solution of

$$\tilde{\gamma} = \left(-1 + \sqrt{1 + 4\tilde{\gamma}_{RT}}\right)/2 \qquad \text{for } \tilde{\gamma}_{RT} > 0, \qquad (43)$$

which is plotted against $\tilde{\gamma}_{RT}$ in Figure 3a. In the limit of $C_m \to 0$, $|\tilde{\gamma}_{RT}|$ (,$|\tilde{\gamma}_{KH}|$) $\ll 1$. It follows that $\tilde{\gamma} \sim \tilde{\gamma}_{RT}$ as mentioned earlier. As is illustrated in Figure 3b, for $\tilde{\gamma}_{RT} > 0$ the growth rate $\tilde{\gamma}$ in equation (43) is smaller than $\tilde{\gamma}_{RT}$, the growth rate of the RT instability without inertial effect. This fact means that the RT instability can be significantly suppressed by the inertial effect, but not extinguished by it.

4.2. Numerical Solution

[24] The solutions to the cubic equation (41) are numerically solved for any set of $\tilde{\gamma}_{RT}$ and $\tilde{\gamma}_{KH}$. Figure 4 shows the growth rate $\tilde{\gamma}$ as a function of $\tilde{\gamma}_{RT}$ and $\tilde{\gamma}_{KH}$, for the fastest growing mode (designated as the first solution). The second solution of $\tilde{\gamma}$ is negative when $\tilde{\gamma}$ is real. The third solution is positive for $\tilde{\gamma}_{RT} < 0$ and $\tilde{\gamma}_{KH} > 1$, but its magnitude is smaller than that of the first solution in Figure 4. In the followings the fastest growing wave solution (Figure 4) is only taken up. Figure 5a shows the ratio of $\tilde{\gamma}(\tilde{\gamma}_{RT}, \tilde{\gamma}_{KH})/\tilde{\gamma}(0, \tilde{\gamma}_{KH})$ for $\tilde{\gamma}_{KH} > 1$, namely, the growth rate of the hybrid mode relative to that of the KH mode. For any value of $\tilde{\gamma}_{KH}$ (>1), the hybrid mode growth rate increases with $\tilde{\gamma}_{RT}$ and vanishes at a certain negative value of $\tilde{\gamma}_{RT}$. Figure 5b shows the ratio of $\tilde{\gamma}(\tilde{\gamma}_{RT}, \tilde{\gamma}_{KH})/\tilde{\gamma}(\tilde{\gamma}_{RT}, 0)$ for $\tilde{\gamma}_{RT} > 0$, namely, the growth rate of the hybrid mode relative to that of the RT mode. For any value of $\tilde{\gamma}_{RT}$ (>0), the hybrid mode growth rate increases with $\tilde{\gamma}_{KH}$. In short, as naturally expected, both drivers of the KH and RT instabilities, namely, the velocity shear and the energy density gradient build up the hybrid instability which is enhanced in comparison to the instability either in the KH or RT mode.

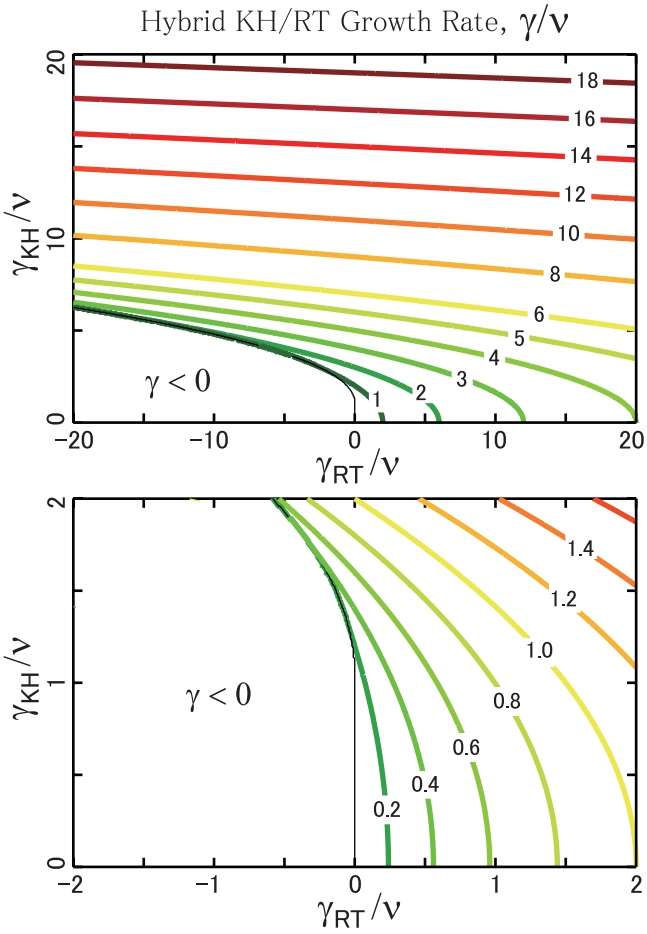

Figure 4. Growth rate of the fastest growing mode: $\tilde{\gamma}$ is shown as a function of $\tilde{\gamma}_{RT}$ and $\tilde{\gamma}_{KH}$. Plot at the top is in the range of $|\tilde{\gamma}_{RT}| \le 20$ and $0 \le \tilde{\gamma}_{KH} \le 20$; the bottom one is an expanded plot for small values of $|\tilde{\gamma}_{RT}|$ and $\tilde{\gamma}_{KH}$. The thin black lines are for demarcation between $\tilde{\gamma} > 0$ and $\tilde{\gamma} < 0$.

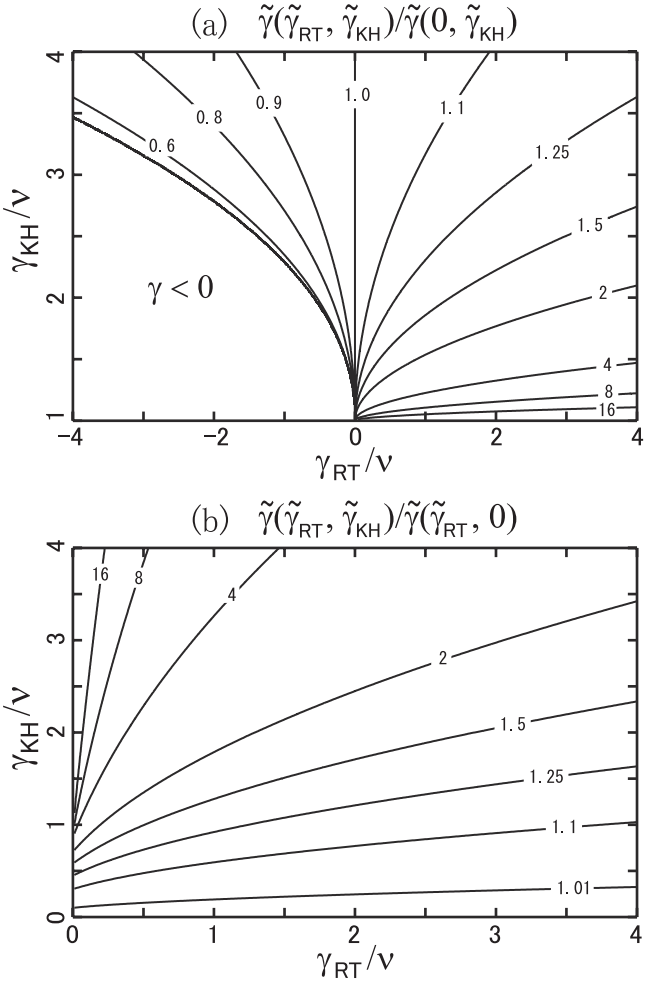

Figure 5. Growth rate of the fastest growing mode: (a) $\tilde{\gamma}(\tilde{\gamma}_{RT}, \tilde{\gamma}_{KH})/\tilde{\gamma}(0, \tilde{\gamma}_{KH})$ for $\tilde{\gamma}_{KH} > 1$ and (b) $\tilde{\gamma}(\tilde{\gamma}_{RT}, \tilde{\gamma}_{KH})/\tilde{\gamma}(\tilde{\gamma}_{RT}, 0)$ for $\tilde{\gamma}_{RT} > 0$ are plotted in the $(\tilde{\gamma}_{RT}, \tilde{\gamma}_{KH})$ space.

[25] As mentioned above, the present analysis is applicable to the case of $k_y L/2 \ll 1$. To assess more precise conditions, first look into Figure 3 of *Michalke* [1964], the plot of the KH growth rate versus the wave number for the hyperbolic tangent velocity profile. The tangent to the growth rate curve at the origin corresponds to the long wavelength approximation, being well fitted to the curve in the range of $k_y L/2 \lesssim 1/4$, where the abscissa is appropriately converted. Similarly, looking into the growth rate of the RT instability for the energy density profile with finite thickness (for example, Figure B1a), the long wavelength approximation is found to be satisfactory for $k_y L/2 \lesssim 1/4$. (Figure B1a shows that for the case of $D \sim 0$, $\gamma/\gamma_{m,0} \sim 0.25$ at $k_y L = 0.5$, equivalently $\gamma \sim \gamma_{RT}$, which is in good agreement with the result of equation (43) in the limit of $C_m \rightarrow 0$.) Thus the results of the present analysis are assumed to be reasonable for wavelengths of $\lambda \gtrsim 4\pi L$. If $\lambda < 4\pi L$, the dispersion relation of (41) will give the positive growth rates greater than the actual ones. Hence the analysis of the hybrid instability using smooth profiles in velocity and energy density should be conducted in the future. Recalling that the scale length L be even greater than the cyclotron radius of auroral protons on the order of kilometers (as mapped to the ionosphere), a requirement of the drift approximation, the condition of $\lambda \gtrsim 100$ km at the ionospheric height is practically imposed on the following discussions.

[26] The inertial relaxation rate ν is evaluated as $\nu > 0.08\ \mathrm{s}^{-1}$ for the main body of the plasma sheet (PS) with $\Sigma_P > 4$ mho and $C_m < 50$ F (see Figures 1a–1c). The main body is here defined as the PS region excepting both the most poleward part with $C_m > 50$ F or $\Sigma_P < 4$ mho and the most equatorward one with $\Sigma_P < 4$ mho. In the present section, the KH/RT stability is discussed only for the PS main body. Application to other regions will be described in section 5.

[27] The growth rate of γ_{KH} is estimated as $\gamma_{KH} \lesssim 0.03\ \mathrm{s}^{-1}$ for long azimuthal wavelength λ of $\gtrsim$100 km and azimuthal flow velocity with a variance $(2\Delta_V)$ of $\lesssim$1 km/s. (In Appendix C the evaluation of a shear frequency is further discussed in comparison with that by *Keskinen et al.* [1988].) Thus in the PS main body γ_{KH} is less than ν for wavelengths of $\gtrsim$100 km, meaning that such waves in the KH mode with $\gamma_{RT} = 0$ cannot grow by itself (see equation (42)). The situation drastically changes when γ_{RT} becomes positive, even if it is much smaller than ν, i.e., $\tilde{\gamma}_{RT} \ll 1$, that is, a hybrid wave can grow with a growth rate of $\sim\gamma_{RT}$, as is seen from Figure 4 or Figure 5b. For small values of $\tilde{\gamma}_{KH} = \gamma_{KH}/\nu \lesssim 0.03/0.08$, the conditions for wave growth in the hybrid mode are similar to those in the RT mode, namely, $\tilde{\gamma}$ is primarily determined by $\tilde{\gamma}_{RT}$, being insensitive to $\tilde{\gamma}_{KH}$ (see those figures). This means that the RT instability is more influential than the KH instability in the stability of large-scale phenomena.

[28] Finally, γ_{RT} is numerically evaluated. The parameter values are chosen as follows. The ionospheric magnetic field, B_i is 6×10^4 nT; the average magnetic drift speed of the plasma sheet protons, $w\nu_m$ is 400 m/s; the flux tube content N is specified by the conditions that the number density of particles, n is 1 cm^{-3} when they are contained in a flux tube with the reference flux tube volume of $B_i R_{B,0} = 1.32 \times 10^7$ km, which is the value for the dipole field line with a geocentric distance of 7 R_E at the equator: $N = nB_i R_{B,0} = 1.32 \times 10^{16}\mathrm{m}^{-2}$. Assuming that the flux tube content is conserved along a convection path, the upper limit of $(\nu_m/R_B^{2/3})\Delta_{\mathcal{E}}$ in the expression of γ_{RT} is approximated by $w\nu_m N$. For $\Sigma_P > 4$ mho and $\lambda \gtrsim 100$ km as assumed above, γ_{RT} is estimated as $\gamma_{RT} \lesssim 0.11\ \mathrm{s}^{-1}$. Then γ_{RT} may reach a value comparable to ν, but in that case the growth time of γ_{RT}^{-1} is shorter than the Alfvén transit time, invalidating the electrostatic approximation. While Figure 3b shows that the maximal inertial effect, around $\gamma_{RT}/\nu \sim 0.11/0.08$, is $\sim$40% reduction of the RT growth rate, the inertial effect is quite small within the electrostatic limit, i.e., for $\gamma_{RT}/\nu < 0.01/0.08$. The effect of particle diffusion may be more important for the RT instability, which is examined in Appendix B, using the energy density profile with a finite gradient in latitude.

5. Application to Auroral Deformations

[29] So far, auroral deformations have often been interpreted exclusively as a result of the KH instability, neglecting the effects of ionospheric current closure and concurrence of the RT instability. Here it is noted that the

both effects are a key to satisfactory understanding of some auroral phenomena.

5.1. Dayside Aurora

[30] Basically it is assumed that the LLBL particle population makes a major contribution to the generation of the region 1 FAC in the LLBL region via the pressure-gradient-driven mechanism [*Yang et al.*, 1994; *Yamamoto et al.*, 2002]. On this line, either of two types of the dayside aurora, the bright spots (BSs) and the radially aligned arcs (RAs) are likely to arise from spatial modulation of the inner boundary of an LLBL particle population [*Yamamoto and Ozaki*, 2005, hereinafter referred to as YO05]. One possible cause of the modulation of the LLBL inner boundary was assumed to be the generation of KH waves therein. Here in view of the hybrid KH/RT stability, this possibility is reexamined.

[31] For long azimuthal wavelength of $\lambda \gtrsim 100$ km and azimuthal flow velocity with a variance of $2\Delta_V \sim 1.5$ km/s [*Sandholt et al.*, 1990], γ_{KH} is estimated as $\gamma_{KH} \sim 0.047 \cdot (100/\lambda)$ s^{-1}, where λ is in kilometer. (The more precise evaluation of the KH growth rate around the LLBL inner boundary was earlier made by, for example, *Ogilvie and Fitzenreiter* [1989] using the ISEE 1 satellite data.)

[32] The inertial relaxation rate is estimated as $\nu \lesssim 0.03$ s^{-1} for $C_m > 200$ F (see Figures 2a and 2b as well as their legend). Note that such high values of C_m come from the heavily loaded flux tubes in the LLBL as assumed in that legend. Thus $\tilde{\gamma}_{KH}$ is found to be $\tilde{\gamma}_{KH} \gtrsim 1.6 \cdot (100/\lambda)$. If $\gamma_{RT} \sim 0$, as is seen from Figure 4 it is possible that KH waves are developed around the LLBL inner boundary. It is also noted that if a sufficiently strong shear appears, the KH instability is excited even in the case of $\gamma_{RT} < 0$ (see Figure 4). Looking into the numerical simulation of KH vortices in the LLBL-ionosphere coupling by *Wei and Lee* [1993], BSs arising from KH waves appear predominantly in the postnoon sector, which could not explain the observations of BSs in the prenoon sector [e.g., *Lui et al.*, 1989]. If the Tsyganenko model [e.g., *Tsyganenko*, 1989] is used in mapping to the ionosphere, the BSs from that simulation might be extended along the "radial direction" (away from the cusp center) so that their shape may be dissimilar to that of the observed BSs, while the deformation depends on where the vortices are formed in the equatorial plane, specifically, the distance to the open/closed boundary. As will be discussed later, the ionospheric projection of fully developed (round) vortices also seems dissimilar to the linear configuration of individual arcs radially aligned.

[33] To evaluate γ_{RT} for the energy density gradient in the LLBL particle population, the parameter values are chosen as follows. A typical value of the average magnetic drift speed of the LLBL protons with $w \sim 200$ eV, $w\nu_m$ is ~50 m/s as inferred from Figure 9 of *Yamamoto et al.* [2002]; the number density of particles, n is 1 cm^{-3} when they are contained in the flux tube at $X = 0$ on the outer boundary of the closed LLBL (termed the cusp line in YO05), the volume of which is $R_B = 33.7R_{B,0}$ (in the *Tsyganenko* [1989] magnetic field model with $Kp = 0$), so that the flux tube content there is given by $N = nB_iR_B = 4.45 \times 10^{17}$m^{-2}. Note that region 1 FACs with observed intensity profiles can be reproduced using such a model of the flux tube (energy) content in the LLBL region [YO05]. For $\Sigma_P \sim 6$ mho and $\lambda \gtrsim 100$ km, γ_{RT} is estimated as $\gamma_{RT[LB]} \sim -0.31 \cdot (100/\lambda)$ s^{-1}, where the minus sign means that the LLBL inner boundary is stable to the RT instability. On the other hand, the plasma sheet (PS) particles may have an inward gradient of the energy density in the region where the LLBL and PS particles are mixed. The associated growth rate of γ_{RT} is estimated using the parameter values given in section 4: $\gamma_{RT[PS]} \sim 0.074 \cdot (100/\lambda)$ s^{-1}, where $\Sigma_P \sim 6$ mho is assumed. The "total growth rate", i.e., the sum of $\gamma_{RT[LB]}$ and $\gamma_{RT[PS]}$ is $\gamma_{RT[T]} \sim -0.24 \cdot (100/\lambda)$ s^{-1}, showing that the LLBL inner boundary is stable to the RT instability in this specific example. However, the observations [e.g., *Sckopke et al.*, 1981; *Le et al.*, 1994, 1996] do not necessarily show that the pressure of the LLBL particles is greater than that of the PS ones. Therefore all the possibilities of $\gamma_{RT[T]} < 0$ and $\gamma_{RT[T]} \gtrsim 0$ need to be considered.

[34] For the above numerical example of $\gamma_{RT[T]} < 0$, $\tilde{\gamma}_{RT}(= \gamma_{RT}/\nu)$ is found to be $\tilde{\gamma}_{RT} \lesssim -8 \cdot (100/\lambda)$. Noting that the ratio of $\tilde{\gamma}_{KH}/\tilde{\gamma}_{RT}$ is independent of C_m, from Figure 4 the LLBL inner boundary is found to be stable to the hybrid KH/RT instability for long wavelength perturbations. It should be emphasized that the boundary can be KH unstable but that instability is suppressed by the RT stabilizing effect acting in the place where the energy density has an outward gradient in latitude. Other candidates for causing spatial modulation of the LLBL inner boundary are assumed to be KH waves at the sheath/LLBL interface [e.g., *Fairfield et al.*, 2000] and surface waves on the magnetopause which could be caused by flux transfer events [*Song et al.*, 1988] or solar wind pressure fluctuations [*Elphic and Southwood*, 1987]. When the LLBL inner boundary is perturbed slightly, as shown in Figure 4 of YO05 (for the case of $\tilde{A}_m = 0.2$), under the influence of those "external" (outside the magnetosphere) waves, space charges are created by different magnetic drifts of ions and electrons around the perturbed boundary, being responsible for the formation of BSs (bright spots), while the resulting $\mathbf{E} \times \mathbf{B}$ drift motion acts to suppress the amplification of the modulation as an RT reacting/stabilizing process (Figure 6a). As studied by YO05, this model can explain the occasional appearance of BSs in the prenoon sector. Such dawn-dusk asymmetry of the BS formation is closely related to the fact that the associated FACs exhibit the dawn-dusk antisymmetry characteristic of the large-scale region 1 currents, as averaged over a couple of wave cycles, owing to the inclination of the unperturbed LLBL inner edge to the direction of the average magnetic drift.

[35] The modulation by external waves can be amplified for the case of $\gamma_{RT[T]} \gtrsim 0$. Suppose that an LLBL is newly formed by sheath plasma entry across the deformed magnetopause boundary (Figure 6b) and that its inner edge has a waveform as shown in Figure 4 of YO05 (for the case of $\tilde{A}_m = 1.0$). According to the numerical model in YO05, RAs will be created as a result of the charge separation in that LLBL population. It is assumed that the effect of such charge separation begins to suppress the boundary deformation when the (flux tube) content of the new LLBL population reaches a significant fraction of that of the ambient plasma. (In the previous model of RAs by YO05, the cause of the modulation of an injection front is assumed to be the small-amplitude ("primary") waves generated in

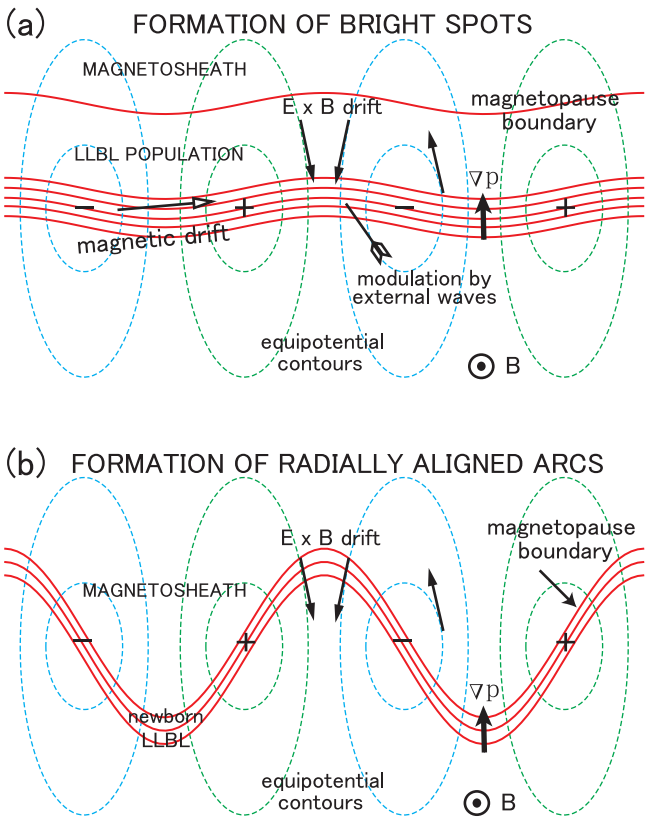

Figure 6. Schematics illustrating possible formations of (a) bright spots (BSs) and (b) radially aligned arcs (RAs). (a) The LLBL inner boundary (striped in red) is slightly modulated under the influence of external waves (not shown). Space charges induced by the magnetic drifts of the LLBL particles, in the region of pressure gradient, can be responsible for the formation of BSs, and at the same time the resulting **E** × **B** drift motion acts to suppress the boundary modulation. The figure is for dusk side. (b) The magnetopause boundary deformation can significantly proceed in a situation that the pressure gradient of the magnetospheric plasma is insignificant. Then an LLBL (striped in red) with a waveshaped boundary is newly created by sheath plasma entry, providing space charges responsible for the RAs. The resulting **E** × **B** drift motion also acts to suppress the deformation.

the LLBL population proper with an outward pressure gradient. However, the sustenance of these waves is incompatible with the modulation growth, namely the associated **E** × **B** drift motion wipes out the primary waves.)

[36] The temporal and spatial development of RAs is predicted as follows (see Figure 7). The front of a chain of external waves propagates antisunward along the magnetopause at a speed of a few hundreds km/s. For a time period of 5 min, the propagation distance is ~10 R_E. Provided that the wavelengths of the external waves are given as shown in Figure 4 of YO05, one to two cycles of RAs are newly created around $X = 0$ during a 5-min period. The inward deformation/progression of a newly formed LLBL near the equator is mapped to the ionosphere, as extension of individual arcs as if they emanated from the cusp (see Figure 10b of YO05), although the statistical field model like Tsyganenko's may not be applicable to the mapping in the case of a highly deformed magnetopause. If the magnetopause boundary deformation proceeds in time as in the KH wave simulation by *Fairfield et al.* [2000], the time required for "full extension" of an RA will be a few hundred seconds. These features are consistent with the observational morphology of developing RAs, Figure 3 of *Elphinstone et al.* [1991]. (The "fan arcs" which are observed, by the Viking ultraviolet imager, predominantly in the morning sector when the IMF (interplanetary magnetic field) B_Z is positive and B_Y is negative [*Elphinstone et al.*, 1991, 1993] may be one specific type of the RAs identified by *Meng and Lundin* [1986] using the DMSP (Defense Meteorological Satellite Program) imagery; they appear both on the evening and morning sides, independently of the IMF B_Z. This fact may partly come from the difference in spatial resolution between the DMSP and Viking auroral images: in the latter a cluster of thin discrete arcs do not seem to be identified.)

[37] For the case of $\gamma_{RT[T]} > 0$, the hybrid waves are likely to be developed around the LLBL inner boundary. If these waves extend to near the open/closed boundary, the resulting auroral pattern, i.e., the ionospheric projection of fully developed (circular) vortices with negative charge looks like a "fan" as a whole, but each "vane" is generally in elliptical shape, being dissimilar to the linear (although winding) configuration of individual arcs in the DMSP images of RAs [*Meng and Lundin*, 1986]. This fact suggests the unlikeliness of $\gamma_{RT[T]} > 0$. Resolving such uncertainty/ambiguity in the relationship between the dayside aurora and the plasma stability is a future task both in observational and theoretical studies on magnetospheric physics.

[38] In summary, the BSs are likely to be formed as a result of the magnetic-drift-induced charge separation acting on the inner boundary of the LLBL particle population with an outward pressure gradient, when it is slightly perturbed by some instability (e.g., KH instability) outside the magnetosphere. The magnetopause boundary could be much more deformed by this external instability if the total pressure gradient of the magnetospheric plasma is insignificant. The RAs are thought to arise from a waveshaped inner edge of an LLBL which may be newly formed by sheath plasma entry across the deformed magnetopause.

5.2. Diffuse Auroral Undulation

[39] According to the simulation model by *Yamamoto et al.* [1993, 1994], some type of the large-amplitude undulation (referred to as the giant undulation in their papers) [e.g., *Lui et al.*, 1982; *Zhang et al.*, 2005] on the equatorward diffuse auroral boundary is assumed to be a result of spatial modulation of the energetic protons by KH waves arising from the polarized arc sheet. The arc sheet is defined as the azimuthally aligned sheet of enhanced density, a product of particle supply from the ionosphere. The polarization is due to anomalous cross-field diffusion of protons in the arc sheet. Here the possibility of the generation of those KH waves is reexamined in the context of the hybrid KH/RT stability with inertial relaxation effect.

[40] The growth rate of a most unstable KH wave in the polarized arc sheet is expressed as $\gamma_{KH} \sim \Delta_V/\lambda$, which is derived from the linear analysis of the KH instability by

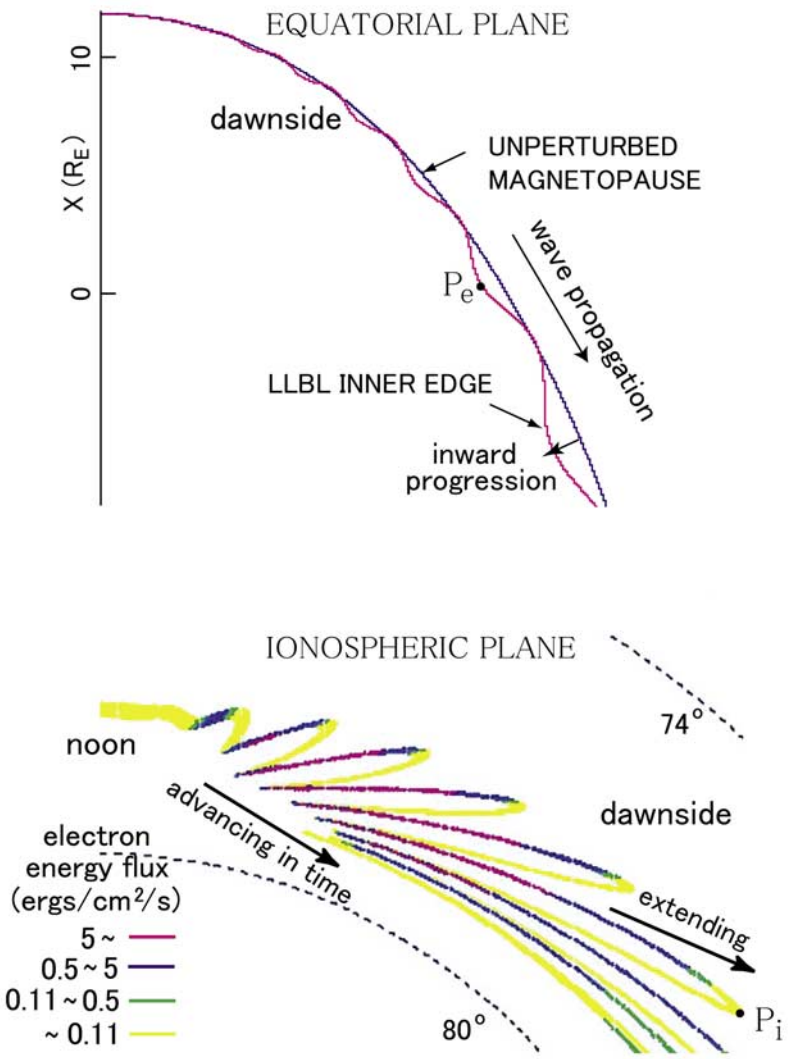

Figure 7. Model for the temporal/spatial development of RAs in the equatorial plane (top) and ionospheric plane (bottom). They are adapted from Figures 4 and 10b of *Yamamoto and Ozaki* [2005]; the dawn side is chosen for comparison with Figure 3 of *Elphinstone et al.* [1991]. Point P_e in the equatorial plane is mapped to P_i in the ionospheric plane.

Ganguli et al. [1988]. The formula for γ_{KH} in equation (39) is not applicable to the present case, because velocity shears arise in a triple layer of space charges, not in a single charge layer assumed in section 4. For wavelength of $\lambda \gtrsim 100$ km and flow velocity with $\Delta_V \sim 1$ km/s, γ_{KH} is estimated as $\gamma_{KH} \sim 0.01 \cdot (100/\lambda)$ s^{-1}. For evaluating γ_{RT}, the parameter values are chosen as follows. A typical value of the average magnetic drift speed of the arc sheet protons with $w \sim$ 200 eV, $w\nu_m$ is ~4 m/s at subauroral latitudes, a value based on the dipole field [see *Yamamoto et al.*, 1991, Figure 6]; the number density of the arc sheet particles, n is 20 cm^{-3} [see *Yamamoto et al.*, 1993, section 6] when they are contained in a flux tube at subauroral latitudes, where $R_B \sim 0.1R_{B,0}$, so that the flux tube content there is given by $N = nB_iR_B \sim 2.64 \times 10^{16}$m^{-2}. For $\Sigma_P \sim 0.5$ mho and $\lambda \gtrsim$ 100 km, γ_{RT} is estimated as $\gamma_{RT} \sim \pm 0.018 \cdot (100/\lambda)$ s^{-1}, where plus and minus signs are for the poleward and equatorward sides of the arc sheet, being unstable and stable to the RT instability, respectively.

[41] Considering the aforementioned density enhancement in the arc sheet, from Figures 1a–1c the capacitance C_m is found to be ~2 F at subauroral latitudes, if the arc sheet is constituted by an H^+ plasma. For an O^+ plasma, $C_m \sim 32$ F. The inertial relaxation rate ν is then in the range between ~0.016 and ~0.25 s^{-1}. Thus $\tilde{\gamma}_{KH}$ and $\tilde{\gamma}_{RT}$ are found to be $0.04 \cdot (100/\lambda) \lesssim \tilde{\gamma}_{KH} \lesssim 0.64 \cdot (100/\lambda)$ and $0.07 \cdot (100/\lambda) \lesssim |\tilde{\gamma}_{RT}| \lesssim 1.2 \cdot (100/\lambda)$, respectively. The polarized arc sheet will be KH stable because of $\nu > \gamma_{KH}$, but not ruling out the possibility that a strong shear of $\gamma_{KH} \sim 0.1$ s^{-1} leads to the excitation of a KH instability. On the contrary, a KH/RT hybrid wave is more likely to grow, on the poleward side of the arc sheet, with a growth rate comparable to γ_{RT}, reflecting the characteristics of the hybrid growth rate for $\tilde{\gamma}_{KH} < 1$ as shown in Figure 4 or Figure 5b. It is then suggested that the hybrid KH/RT instability, rather than the KH instability, plays an important role in the modulation of energetic protons, leading to the

formation of some type of the large-amplitude undulation on the equatorward diffuse auroral boundary.

6. Conclusions

[42] A linear analysis of the hybrid KH/RT instability is conducted for an electrostatic magnetosphere-ionosphere coupling system. For reassessment of the KH stability, the inertial capacitance C_m in the magnetosphere is evaluated using the Tsyganenko model, under the conservation of a flux tube content. On the basis of the calculated profile of C_m, the following facts are identified. So far as long wavelength ($\gtrsim$100 km) perturbations are concerned, the main body of the plasma sheet is KH stable because the inertial relaxation rate is greater than the shear frequency. On the contrary, the hybrid KH/RT instability can occur at places where the energy density of plasma sheet particles has an inward gradient. As for the inner boundary of the low-latitude boundary layer, it is found stable to the hybrid instability when the outward pressure gradient of the LLBL particles dominates the inward one of the plasma sheet particles. In this situation the bright spots can be produced by the magnetic-drift-induced charge separation on the LLBL inner boundary, if the boundary is slightly perturbed externally, i.e., by some instability outside the magnetosphere, not by KH waves inside it. Under the conditions that the total pressure of the magnetospheric plasma is insignificant, the magnetopause boundary can be more readily deformed by the external instability. In this situation, the RAs are likely to appear as the ionospheric projection of the waveshaped inner edge of an LLBL which is newly created by sheath plasma entry across the deformed magnetopause. In addition, it is suggested that the hybrid KH/RT instability may be responsible for some type of the large-amplitude undulation as is occasionally observed on the equatorward boundary of a diffuse aurora.

Appendix A

[43] The conditions for the approximations used in the derivation of the dispersion relation of (41), in sections 2 through 4, are discussed in the following items 1–3.

[44] 1. Because the ionospheric field $\boldsymbol{B}_i$ is well approximated by the dipole field, $dB_i/R_E d\theta \simeq (B_i/R_E)3 \sin\theta \cos\theta/(1 + 3\sin^2\theta)$, where θ is the latitude. In the auroral zone $dB_i/R_E d\theta \approx (1/3)(B_i/R_E)$, meaning that the scale length for $\nabla_\perp B_i$ is $\sim 3R_E$. On the other hand, div $\boldsymbol{V}_E \simeq -2\boldsymbol{V}_E \cdot \nabla B_i/B_i$ and div $\boldsymbol{\nu}_m \simeq -2\boldsymbol{\nu}_m \cdot \nabla B_i/B_i$ are derived using rot$\boldsymbol{E} = 0$ and rot$\boldsymbol{B}_i = 0$ in the ionospheric plane. Hence div $N^P\boldsymbol{V}_E = N^P$div $\boldsymbol{V}_E + \boldsymbol{V}_E \cdot \nabla N^P \simeq -2N^P\boldsymbol{V}_E \cdot \nabla B_i/B_i + \boldsymbol{V}_E \cdot \nabla N^P$ and div $wN^P\boldsymbol{\nu}_m = wN^P$div $\boldsymbol{\nu}_m + \boldsymbol{\nu}_m \cdot \nabla(wN^P) \simeq -2wN^P\boldsymbol{\nu}_m \cdot \nabla B_i/B_i + \boldsymbol{\nu}_m \cdot \nabla(wN^P)$. It is immediately found that on the right-hand side of each of these two equations, the first term is negligible compared with the second term for any type of auroral disturbance. This fact assures the derivation of equation (13). Thus the expressions of div $\boldsymbol{V}_E = 0$ and div $\boldsymbol{\nu}_m = 0$ are allowed in a practical sense.

[45] 2. The ratio of $|\boldsymbol{\Gamma}^p_{in}|/|\boldsymbol{\Gamma}^p_E|$ is reduced to $|C_m d\boldsymbol{E}/dt|/|eN^p\boldsymbol{V}_E|$, using equation (16). It is then estimated as $|\boldsymbol{\Gamma}^p_{in}|/|\boldsymbol{\Gamma}^p_E| < 4 \times 10^{-4} C_m(F)$ for $d/dt < 10^{-2}$ s^{-1} and $N^p \gtrsim 10^{16}$ m^{-2} (see section 4). Therefore in the adiabatic region of the PS (see Figures 1a–1c), $\boldsymbol{\Gamma}^p_{in}$ may be neglected in the derivation of equation (13). For the LLBL with $d/dt < 10^{-2}$ s^{-1} and $N \sim 4 \times 10^{17}$ m^{-2} (section 5.1), $|\boldsymbol{\Gamma}^p_{in}|/|\boldsymbol{\Gamma}^p_E| < 10^{-5} C_m(F)$. Hence in most part of the LLBL region (see Figure 2a), $\boldsymbol{\Gamma}^p_{in}$ may be neglected compared with $\boldsymbol{\Gamma}^p_E$.

[46] 3. The diffusion rate (D/w) will be governed by the intensity level of wave turbulence such as the Alfvén wave noise [e.g., *Lundin et al.*, 1990] and the broadband electrostatic noise [e.g., *Gurnett and Frank*, 1977; *Matsumoto et al.*, 1994], which are assumed responsible for anomalous cross-field diffusion of aurora protons [*Yamamoto et al.*, 1997b]. Because of scarcity of satellite data on such wave turbulence, it is extremely difficult to infer the latitudinal/longitudinal distribution of the diffusion rate averaged over a whole flux tube. Also, in regions relatively near the open/closed boundary, the scale length for the latitudinal variation of $R_B^{2/3}$ may be comparable to the wavelength under study. Hence this variation cannot always be neglected in the derivation of equation (15). Keeping these limitations of the analysis in mind, the diffusion effect in a simplest form is taken up by assuming a "uniform background medium".

Appendix B

[47] The dispersion relation for the RT mode instability without inertial effect is derived for the energy density profile with a finite gradient in latitude. The differential equation suited for the RT mode is written as

$$\frac{d^2\delta\phi(x)}{dx^2} = k_y^2 \left\{ 1 - \frac{\gamma_m(x)}{\gamma + D\left(k_y^2 - \delta\mathcal{E}^{*\prime\prime}(x)/\delta\mathcal{E}^*(x)\right)} \right\} \delta\phi(x), \tag{B1}$$

which is obtained by substituting equation (25) into equation (26) and taking $\omega = k_y V_t + i\gamma$ under the assumption of $V_t = const$, where the diffusion term is retained in equation (25) and the terms containing ν on the left-hand side of equation (26) are only retained in the limit of $C_m \to 0$. Consider a two-dimensional system in the x-y plane: $\gamma_m(x)$, i.e., $-(e\nu_m/B_i\Sigma_P R_B^{2/3})\mathcal{E}^{*\prime}_0(x)$ has a constant value of $\gamma_{m,0}$ (>0) inside the strip of $|x| < L/2$ and vanishes outside it, namely, $\mathcal{E}^*_0(x)$ has a constant gradient ($\mathcal{E}^{*\prime}_0(x) < 0$) only in the strip. In addition, D is assumed constant there.

[48] If $\delta\mathcal{E}^*(x)$ is proportional to cos $k_x x$ or sin $k_x x$ in the range of $|x| < L/2$, equation (B1) has the same type of solution, i.e., $\delta\phi(x) \propto$ cos $k_x x$ or sin $k_x x$, because the quantity in the curly bracket on its right-hand side is constant there. Here note that the solution of $\delta\phi_0(x) \propto$ sin $k_x x$ may be inappropriate because normally such an antisymmetric (with respect to $x = 0$) potential is not seen in numerical simulations of the RT instability. Thus $\delta\phi(x) \propto$ cos $k_x x$. Equation (26) without inertial terms then requires that $\delta\mathcal{E}^*(x) \propto$ cos $k_x x$. Now, equation (B1) takes the following forms inside and outside of the strip of $|x| < L/2$:

$$\frac{d^2\delta\phi(x)}{dx^2} = k_y^2 \left\{ 1 - \frac{\gamma_{m,0}}{\gamma + D\left(k_y^2 + k_x^2\right)} \right\} \delta\phi(x) \tag{B2}$$

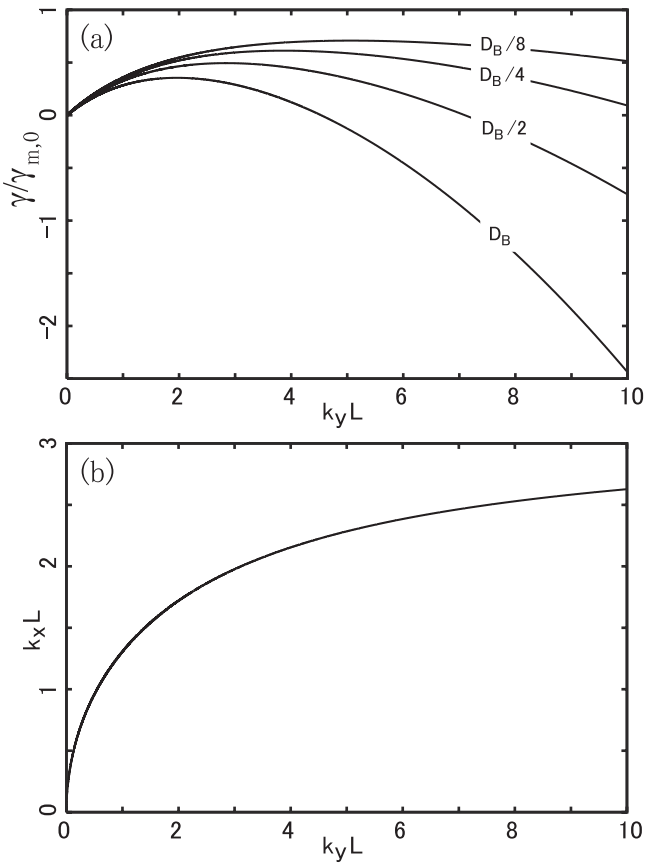

Figure B1. (a) Growth rate of the RT instability: $\gamma/\gamma_{m,0}$ is plotted against the azimuthal wave number $\tilde{k}_y = k_yL$, for various values of α representing different levels of anomalous cross-field diffusion of protons, i.e., $D = D_B$, $D_B/2$, $D_B/4$ and $D_B/8$, where the scale length L is taken to be 100 km and $\gamma_{m,0}$ is the maximum growth rate which is attained as $\tilde{k}_y$ approaches infinity in the case of no diffusion effect. (b) Relation of (B5) between $\tilde{k}_x$ and $\tilde{k}_y$.

and

$$\frac{d^2\delta\phi(x)}{dx^2} = k_y^2\delta\phi(x), \tag{B3}$$

respectively. The solutions to equations (B2) and (B3) are expressed as $\delta\phi(x) = a_0 \cos k_x x$ and $\delta\phi(x) = a_1 \exp(-k_y|x|)$, respectively. From equation (B2), the growth rate γ is related to the wave numbers k_x and k_y as

$$\gamma = \gamma_{m,0}\frac{k_y^2}{k_x^2 + k_y^2} - D\left(k_x^2 + k_y^2\right). \tag{B4}$$

The requirement that $\delta\phi(x)$ and its derivative with respect to x be continuous at $L/2$ and $-L/2$ gives the following relation between k_x and k_y:

$$k_y = k_x \tan(k_xL/2). \tag{B5}$$

For a given k_y (>0), an infinite number of k_x (>0) are determined as the solutions of the above equation. They are labeled as $k_x^1, k_x^2, \ldots, k_x^n, \ldots$, i.e., $(n-1)\pi < k_x^nL/2 < (n-1/2)\pi$. From the k_x dependence of γ in equation (B4), the growth rate is found to be smaller for a higher harmonic number n. For this reason, hereafter the analysis is limited to the fundamental mode with $n = 1$.

[49] The perturbation profile of $\delta\mathcal{E}^*$ in the range of $|x| < L/2$ is now written as

$$\delta\mathcal{E}^* = -a_0\frac{R_B^{2/3}\Sigma_P}{e\,\nu_m}\frac{k_x^2 + k_y^2}{k_y}\exp\gamma t\cos k_x x\sin k_y(y - V_t t), \tag{B6}$$

and $\delta\mathcal{E}^* = 0$ for $|x| > L/2$, which are obtained from equation (26). In comparison with $\delta\phi = a_0 \exp\gamma\, t \cos k_x x \cos k_y\,(y - V_t t)$, $\delta\mathcal{E}^*$ has a phase difference of $\pi/2$ in the y-direction so that a (positive) peak of $\delta\phi$ lies at a point where $-\partial\delta\mathcal{E}^*/\partial y$ maximizes, the same way as predicted from the associated charge separation.

[50] Equation (B4) is rewritten in terms of the nondimensional wave numbers $\tilde{k}_x$ and $\tilde{k}_y$ which are defined as $\tilde{k}_x = k_xL$ and $\tilde{k}_y = k_yL$, respectively:

$$\frac{\gamma}{\gamma_{m,0}} = \frac{\tilde{k}_y^2}{\tilde{k}_x^2 + \tilde{k}_y^2} - \frac{\alpha D_B}{L^2\gamma_{m,0}}\left(\tilde{k}_x^2 + \tilde{k}_y^2\right), \tag{B7}$$

where D_B is the Bohm diffusion rate at the ionospheric height, i.e., $(2w/3)/16eB_i$; the diffusion rate for the ionospheric projections of protons in the magnetosphere may be scaled in terms of D_B, i.e., $D = \alpha D_B$ for $\alpha \lesssim 1$ (see Appendix C of YI04). Taking $w = 8$ keV, $L = 100$ km, and $\Sigma_P = 8$ mho, as well as the same values of parameters B_i, N, and $w\nu_m$ as used in the evaluation of γ_{RT} (section 4), $\gamma_{m,0}$, i.e., $(e/B_i\Sigma_P)\,(w\nu_m N/L)$ is estimated as $\sim 1.8 \times 10^{-2}$ s^{-1} and $D_B/L^2\gamma_{m,0}$ is $\sim 3.2 \times 10^{-2}$. Figure B1a illustrates the growth rates γ for various values of α as functions of $\tilde{k}_y$, using the relation of (B5) between $\tilde{k}_x$ and $\tilde{k}_y$, which is also plotted in Figure B1b. The growth rate for a given diffusion rate maximizes at a certain value of the azimuthal wavelength ($\lambda_{\max}$), which depends on the diffusion rate. If the width L is changed while the other parameter values are fixed, the maximum growth rate can be estimated as a function of L, which is shown in Figure B2a. The wavelength $\lambda_{\max}$ corresponding to the maximum growth is shown in Figure B2b. All the curves are truncated at $L = 25$ km because the drift approximation used in the present analysis requires that the scale length L should be much greater than the ion cyclotron radius (a few kilometers) projected to the ionosphere. Note that the RT instability is suppressed for a short wavelength perturbation by the finite cyclotron radius effect of ions [*Lehnert*, 1961; *Roberts and Taylor*, 1962; *Huba*, 1996b].

[51] Figure B1a indicates that the cross-field diffusion of particles acts to suppress the wave growth particularly when the (azimuthal) wavelengths are sufficiently short. (Note that k_x increases with k_y.) This fact can be physically understood by noting that the particle diffusion tends to smooth out energy density perturbations. In this context, recall the previous theoretical predictions that owing to the low-frequency wave turbulence such as the broadband electrostatic noise and the Alfvén wave noise, the anomalous cross-field diffusion coefficient averaged over a flux tube, for plasma sheet protons, is likely to reach a significant fraction of the Bohm rate at least in disturbed periods

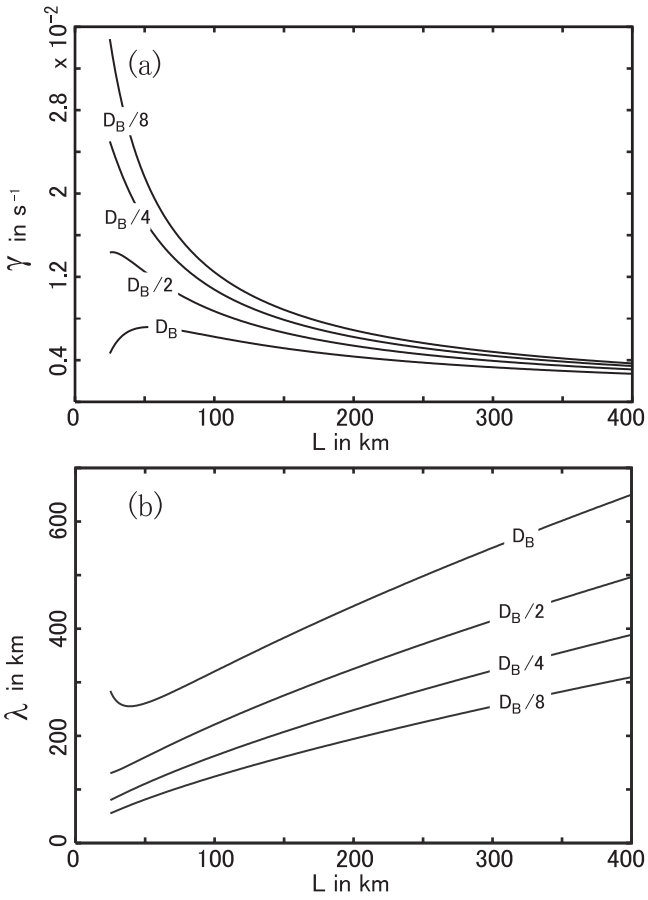

Figure B2. (a) Maximum growth rates of the RT instability are plotted as functions of L (in km), for various values of α. (b) Wavelength λ_{max} (in km) corresponding to the maximum growth.

[*Yamamoto et al.*, 1997b] and that charge separation induced by such diffusion may be responsible for the generation of region 0 FACs near the poleward edge of the auroral oval [YI04].

[52] In summary, auroral disturbances with a typical wavelength of a few hundred kilometers are likely to grow by the RT instability at the places of inward energy density gradient in the plasma sheet, when the cross-field diffusion rate of protons is a significant fraction of the Bohm rate. An additional condition for the emergence of visible disturbances is that the growth time of the RT instability is shorter than the time required for particles, with a radial drift velocity of $\approx$0.1 km/s, to transit over the unstable region of $\approx$100 km in width, that is a time of $\approx 10^3$ s, provided that the unstable region is standing.

Appendix C

[53] A brief comparison is made between the present work and that by *Keskinen et al.* [1988] in the evaluation of a growth rate of the KH instability in the M-I coupling system. They assumed an equilibrium configuration throughout the ionosphere and the magnetosphere as follows: The Pedersen conductivity Σ_P and the inertial capacitance C_m are both proportional to the field-line-integrated density N, defined as $\int ndz$, implying that the average density in the magnetosphere is roughly proportional to the ionospheric one. The $\mathbf{E} \times \mathbf{B}$ drift velocity, $\boldsymbol{V}$ has only a longitudinal (y-)component which varies with x as $V_y(x) = -V_0 \tanh(x/L)$, where the coordinates x and y are reverse to those in their paper. There is no polarization current because the gradient of E_x is perpendicular to $\boldsymbol{V}$. In this configuration the divergence of the Pedersen current is required to be zero:

$$\mathrm{div}\, \Sigma_P(\boldsymbol{E} + \boldsymbol{V}_n \times \boldsymbol{B}) = 0, \tag{C1}$$

where $\boldsymbol{V}_n$ is the neutral wind velocity. Under the assumption that the neutral wind has only a constant y-component V_n, from the above equation the profile of $N(x)$ is derived as

$$N(x) = \frac{N(-\infty)(V_0 - V_n)}{-V_0 \tanh(x/L) - V_n} \tag{C2}$$

so that

$$V_0 = -V_n \frac{N_{\max} - N_{\min}}{N_{\max} + N_{\min}}, \tag{C3}$$

where $N_{\max}$ and $N_{\min}$ denote the maximum and minimum values of $N(x)$, i.e., $N(\infty)$ and $N(-\infty)$, respectively, for the case of $V_0 > 0$ and $V_n < 0$ as assumed in that paper. Note that the existence of a sheared plasma flow as well as its magnitude entirely depend on the neutral wind velocity and the gradient of the integrated density, and that the plasma flow speed is limited to the neutral wind speed. These features are unusual from a viewpoint that the large-scale plasma flows are primarily controlled by charge separation processes in the magnetosphere, which are manifested by the appearance of FACs.

[54] On the contrary, the present paper assumes an equilibrium state of the M-I coupling system such that the magnetospheric charge separation producing large-scale FACs is short-circuited by the ionospheric Pedersen current. Specifically, the equilibrium state for the magnetic-drift-induced FACs is described as

$$\mathrm{div}\, \Sigma_P \boldsymbol{E} = -e R_B^{-2/3} \boldsymbol{\nu}_m \cdot \nabla \mathcal{E}_0^*. \tag{C4}$$

Large-scale FACs, typically the region 1/region 2 FACs, are generated owing to a (small) y-component of $\nabla \mathcal{E}_0^*$ as studied by YI04. In the present work the KH stability is studied under the condition of (C4), free of the severe constraint of (C2) or (C3).

[55] Parameter values that were used in applying the stability criteria to the actual auroral phenomena in the plasma sheet [*Keskinen et al.*, 1988, section 6] need to be reassessed. For the evaluation of the inertial capacitance C_m, the same number density of 1 cm^{-3} was assumed both for the outer and inner plasma sheets. This choice may lead to overestimate of C_m, say 600 F, in the outer plasma sheet, because the local density is decreased in a flux tube of greater volume under the conservation of a flux tube content in the convective transport. A more reasonable estimate of C_M using that conservation law in the Tsyganenko model field [*Tsyganenko*, 1989] is shown in Figures 1a–1c. In the

outer plasma sheet, except for nonadiabatic regions [*Büchner and Zelenyi*, 1989] with $B < 1$ nT in the tail current sheet, normally C_m will be less than 100 F.

[56] The shear frequency V_0/L can be estimated, without specifying values of V_0 and L, for any auroral structure associated with an intense large-scale upward FAC, provided that Σ_P is uniform. Suppose that an FAC with average current density $J_\parallel$ flows out of a longitudinally extended zone in the ionospheric plane. From the integration of equation (20) along a meridian, the shear frequency at the ionospheric height is expressed as $J_\parallel/B_i\Sigma_P$, independently of a latitudinal thickness of the current zone. (In the nighttime plasma sheet, the shear frequency at high altitudes is smaller than the ionospheric one because of anisotropy of the field-line mapping with a greater factor in radial dimension.) The current density $J_\parallel$ from a high-altitude electron population with density n and thermal energy K_{th} is related to the associated field-aligned potential drop, $\Delta\phi$, as $J_\parallel = K\Delta\phi$ [*Knight*, 1973], under the conditions $1 \ll e\Delta\phi/K_{th} \ll B_i/B_a$, where $K = e^2n/(2\pi m_e K_{th})^{1/2}$, m_e is the electron mass, and B_a is the magnetic field strength at the top of the field-aligned acceleration region. Under the same conditions the precipitating electron energy flux $\epsilon_\parallel$ is expressed as $\epsilon_\parallel = K\Delta\phi^2$ [*Lundin and Sandahl*, 1978]. The conductivity Σ_P varies with $\epsilon_\parallel$ as Σ_P (mho) = 0.5 + 160 $\epsilon_\parallel^{1/2}$ [*Harel et al.*, 1981]. From combination of these three relations, the shear frequency is expressed as $V_0/L = K^{1/2}/160B_i = 1.7 \times 10^{-2}n^{1/2}K_{th}^{-1/4}$, where the first term in the expression of Σ_P is neglected, n is in units of per cubic centimeter, and K_{th} in electron volt. Interestingly, the shear frequency under the above conditions only depends on the properties of pre-accelerated electrons carrying a current. Its typical value is 3.8×10^{-3} s^{-1} assuming $n = 1$ cm^{-3} and $K_{th} = 400$ eV [*Lyons*, 1981]. On the other hand, the inertial relaxation rate ν is greater than $\sim$0.08 in the main body of the PS with $C_m < 50$ F and $\Sigma_P > 4$ mho. Then, as already stated in section 4, large-scale auroral structures there are normally stable to the KH instability because $\nu > V_0/L$. This conclusion is in contrast with the suggestion by *Keskinen et al.* [1988] that the outer plasma sheet is likely to be unstable to the KH instability.

[57] **Acknowledgments.** The numerical computation was performed using the SR11000 at the Information Technology Center, University of Tokyo, Tokyo. The present work was supported in part by the joint research programs at the Research Institute for Sustainable Humanosphere, Kyoto University, Uji, Kyoto.

[58] Wolfgang Baumjohann thanks Hiroshi Hasegawa and another reviewer for their assistance in evaluating this paper.

References

Axford, W. I., and C. O. Hines (1961), A unifying theory of high-latitude geophysical phenomena and geomagnetic storms, *Can. J. Phys.*, *39*, 1433–1464.

Büchner, J., and L. M. Zelenyi (1989), Regular and chaotic charged particle motion in magnetotaillike field reversals: 1. Basic theory of trapped motion, *J. Geophys. Res.*, *94*, 11,821–11,842.

Chang, D. B., L. D. Pearlstein, and M. N. Rosenbluth (1965), On the interchange stability of the Van Allen belt, *J. Geophys. Res.*, *70*, 3085–3097.

Elphic, R. C., and D. J. Southwood (1987), Simultaneous measurements of the magnetopause and flux transfer events at widely separated sites by AMPTE UKS and ISEE 1 and 2, *J. Geophys. Res.*, *92*, 13,666–13,672.

Elphinstone, R. D., J. S. Murphree, L. L. Cogger, D. Hearn, and M. G. Henderson (1991), Observations of changes to the auroral distribution prior to substorm onset, in *Magnetospheric Substorms*, *Geophys. Monogr. Ser.*, vol. 64, edited by J. R. Kan et al., pp. 257–275, AGU, Washington, D. C.

Elphinstone, R. D., D. J. Hearn, J. S. Murphree, L. L. Cogger, M. L. Johnson, and H. B. Vo (1993), Some UV dayside auroral morphologies, in *Auroral Plasma Dynamics*, *Geophys. Monogr. Ser.*, vol. 80, edited by R. Lysak, pp. 31–45, AGU, Washington, D. C.

Fairfield, D. H., A. Otto, T. Mukai, S. Kokubun, R. P. Lepping, J. T. Steinberg, A. J. Lazarus, and T. Yamamoto (2000), Geotail observations of the Kelvin-Helmholtz instability at the equatorial magnetotail boundary for parallel northward fields, *J. Geophys. Res.*, *105*, 21,159–21,174, doi:10.1029/1999JA000316.

Farrugia, C. J., F. T. Gratton, L. Bender, H. K. Biernat, N. V. Erkaev, J. M. Quinn, R. B. Torbert, and V. Dennisenko (1998), Charts of joint Kelvin-Helmholtz and Rayleigh-Taylor instabilities at the dayside magnetopause for strongly northward interplanetary magnetic field, *J. Geophys. Res.*, *103*, 6703–6728, doi:10.1029/97JA03248.

Ganguli, G., Y. C. Lee, and P. J. Palmadesso (1988), Kinetic theory for electrostatic waves due to transverse velocity shears, *Phys. Fluids*, *31*, 823–838.

Goertz, C. K., and W. Baumjohann (1991), On the thermodynamics of the plasma sheet, *J. Geophys. Res.*, *96*, 20,991–20,998.

Gurnett, D. A., and L. A. Frank (1977), A region of intense plasma wave turbulence on auroral field lines, *J. Geophys. Res.*, *82*, 1031–1050.

Hallinan, T. J., and T. N. Davis (1970), Small-scale auroral arc distortions, *Planet. Space Sci.*, *18*, 1735–1744.

Harel, M., R. A. Wolf, P. H. Reiff, R. W. Spiro, W. J. Burke, F. J. Rich, and M. Smiddy (1981), Quantitative simulation of a magnetospheric substorm: 1. Model logic and overview, *J. Geophys. Res.*, *86*, 2217–2241.

Huba, J. D. (1996a), The Kelvin-Helmholtz instability: Finite Larmor radius magnetohydrodynamics, *Geophys. Res. Lett.*, *23*, 2907–2910.

Huba, J. D. (1996b), Finite Larmor radius magnetohydrodynamics of the Rayleigh-Taylor instability, *Phys. Plasmas*, *3*, 2523–2532.

Hysell, D. L., and E. Kudeki (2004), Collisional shear instability in the equatorial F region ionosphere, *J. Geophys. Res.*, *109*, A11301, doi:10.1029/2004JA010636.

Iijima, T., and T. A. Potemra (1978), Large-scale characteristics of field-aligned currents associated with substorms, *J. Geophys. Res.*, *83*, 599–615.

Kaufmann, R. L., D. J. Larson, P. Beidl, and C. Lu (1993), Mapping and energization in the magnetotail, *J. Geophys. Res.*, *98*, 9307–9320.

Keskinen, M. J., H. G. Mitchell, J. A. Fedder, P. Satyanarayana, S. T. Zalesak, and J. D. Huba (1988), Nonlinear evolution of the Kelvin-Helmholtz instability in the high-latitude ionosphere, *J. Geophys. Res.*, *93*, 137–152.

Knight, S. (1973), Parallel electric fields, *Planet. Space Sci.*, *21*, 741–750.

Le, G., C. T. Russell, and J. T. Gosling (1994), Structure of the magnetopause for low Mach number and strongly northward interplanetary magnetic field, *J. Geophys. Res.*, *99*, 23,723–23,734.

Le, G., C. T. Russell, J. T. Gosling, and M. F. Thomsen (1996), ISEE observations of low-latitude boundary layer for northward interplanetary field: Implications for cusp reconnection, *J. Geophys. Res.*, *101*, 27,239–27,249.

Lehnert, B. (1961), Stability of a plasma boundary in a magnetic field, *Phys. Fluids*, *4*, 847–854.

Lotko, W., and M.-M. Shen (1991), On large-scale rotational motions and energetics of auroral shear layers, *J. Geophys. Res.*, *96*, 9549–9565.

Lotko, W., B. U. Ö. Sonnerup, and R. L. Lysak (1987), Nonsteady boundary layer flow including ionospheric drag and parallel electric fields, *J. Geophys. Res.*, *92*, 8635–8648.

Lui, A. T. Y., C.-I. Meng, and S. Ismail (1982), Large-amplitude undulations on the equatorward boundary of the diffuse aurora, *J. Geophys. Res.*, *87*, 2385–2400.

Lui, A. T. Y., D. Venkatesan, and J. S. Murphree (1989), Auroral bright spots on the dayside oval, *J. Geophys. Res.*, *94*, 5515–5522.

Lundin, R., and I. Sandahl (1978), Some characteristics of the parallel electric field acceleration of electrons over discrete auroral arcs as observed from two rocket flights, in *Symposium on European Rocket Research*, *ESA SP-135*, p. 125, Eur. Space Agency, Paris.

Lundin, R., G. Gustafsson, A. I. Eriksson, and G. Marklund (1990), On the importance of high-altitude low-frequency electric fluctuations for the escape of ionospheric ions, *J. Geophys. Res.*, *95*, 5905–5919.

Lyons, L. R. (1981), Discrete aurora as the direct result of an inferred high-altitude generating potential distribution, *J. Geophys. Res.*, *86*, 1–8.

Lysak, R. L., Y. Song, and J. C. Grieger (1995), Coupling of the magnetopause to the ionosphere by means of Alfvén waves and field-aligned currents, in *Physics of the Magnetopause*, *Geophys. Monogr. Ser.*, vol. 90, edited by P. Song, B. U. Ö. Sonnerup, and M. F. Thomsen, pp. 385–393, AGU, Washington, D. C.

Matsumoto, Y., and M. Hoshino (2006), Turbulent mixing and transport of collisionless plasmas across a stratified velocity shear layer, *J. Geophys. Res.*, *111*, A05213, doi:10.1029/2004JA010988.

Matsumoto, H., H. Kojima, T. Miyatake, Y. Omura, M. Okada, I. Nagano, and M. Tsutsui (1994), Electrostatic solitary waves (ESW) in the magnetotail: BEN wave forms observed by GEOTAIL, *Geophys. Res. Lett.*, *21*, 2915–2918.

Meng, C.-I., and R. Lundin (1986), Auroral morphology of the midday oval, *J. Geophys. Res.*, *91*, 1572–1584.

Michalke, A. (1964), On the inviscid instability of the hyperbolic-tangent velocity profile, *J. Fluid Mech.*, *19*, 543–556.

Miura, A. (1995), Kelvin-Helmholtz instability at the magnetopause: Computer simulations, in *Physics of the Magnetopause*, *Geophys. Monogr. Ser.*, vol. 90, edited by P. Song, B. U. Ö. Sonnerup, and M. F. Thomsen, pp. 285–291, AGU, Washington, D. C.

Miura, A., and J. R. Kan (1992), Line-tying effects on the Kelvin-Helmholtz instability, *Geophys. Res. Lett.*, *15*, 1611–1614.

Miura, A., and T. Sato (1978), Shear instability: Auroral arc deformation and anomalous momentum transport, *J. Geophys. Res.*, *83*, 2109–2117.

Mozer, F. S., and A. Hull (2001), Origin and geometry of upward parallel electric fields in the auroral acceleration region, *J. Geophys. Res.*, *106*, 5762–5778.

Murphree, J. S., M. L. Johnson, L. L. Cogger, and D. J. Hearn (1994), Freja UV imager observations of spatially periodic auroral distortions, *Geophys. Res. Lett.*, *21*, 1887–1890.

Ogilvie, K. W., and R. J. Fitzenreiter (1989), The Kelvin-Helmholtz instability at the magnetopause and inner boundary layer surface, *J. Geophys. Res.*, *94*, 15,113–15,123.

Pontius, D. H., Jr., and R. A. Wolf (1990), Transient flux tubes in the terrestrial magnetosphere, *Geophys. Res. Lett.*, *17*, 49–52.

Richmond, A. D. (1973), Self-induced motions of thermal plasma in the magnetosphere and the stability of the plasmapause, *Radio Science*, *8*, 1019–1027.

Roberts, K. V., and J. B. Taylor (1962), Magnetohydrodynamic equations for finite Larmor radius, *Phys. Rev. Lett.*, *8*, 197–198.

Sandholt, P. E., M. Lockwood, T. Oguti, S. W. Cowley, K. S. C. Freeman, B. Lybekk, A. Egeland, and D. M. Willis (1990), Midday auroral breakup events and related energy and momentum transfer from the magnetosheath, *J. Geophys. Res.*, *95*, 1039–1060.

Sckopke, N., G. Paschmann, G. Haerendel, B. U. Ö. Sonnerup, S. J. Bame, T. G. Forbes, E. W. Hones Jr., and C. T. Russell (1981), Structure of the low-latitude boundary layer, *J. Geophys. Res.*, *86*, 2099–2110.

Song, P., R. C. Elphic, and C. T. Russell (1988), ISEE 1 & 2 observations of the oscillating magnetopause, *Geophys. Res. Lett.*, *15*, 744–747.

Southwood, D. J., and M. G. Kivelson (1987), Magnetospheric interchange instability, *J. Geophys. Res.*, *92*, 109–116.

Southwood, D. J., and M. G. Kivelson (1989), Magnetospheric interchange motions, *J. Geophys. Res.*, *94*, 299–308.

Tsyganenko, N. A. (1989), A magnetospheric magnetic field model with a warped tail current sheet, *Planet. Space Sci.*, *37*, 5–20.

Vasyliunas, V. M. (1970), Mathematical models of magnetospheric convection and its coupling to the ionosphere, in *Particles and Fields in the Magnetosphere*, edited by B. M. McCormac, pp. 60–71, D. Reidel, Norwell, Mass.

Wagner, J. S., R. D. Sydora, T. Tajima, T. J. Hallinan, L. C. Lee, and S.-I. Akasofu (1983), Small-scale auroral arc deformations, *J. Geophys. Res.*, *88*, 8013–8019.

Walker, A. D. M. (1981), The Kelvin-Helmholtz instability in the low-latitude boundary layer, *Planet. Space Sci.*, *29*, 1119–1133.

Wei, C. Q., and L. C. Lee (1993), Coupling of magnetopause-boundary layer to the polar ionosphere, *J. Geophys. Res.*, *98*, 5707–5725.

Wolf, R. A. (1983), The quasi-static (slow-flow) region of the magnetosphere, in *Solar-Terrestrial Physics*, edited by R. L. Carovillano and J. M. Forbes, pp. 303–368, D. Reidel, Norwell, Mass.

Yamamoto, T., and S. Inoue (2004), Numerical simulation of the combined system of nighttime region 0, region 1 and region 2 field-aligned currents, *J. Geophys. Res.*, *109*, A12223, doi:10.1029/2003JA010272.

Yamamoto, T., and M. Ozaki (2005), A numerical model of the dayside aurora, *J. Geophys. Res.*, *110*, A05215, doi:10.1029/2004JA010786.

Yamamoto, T., K. Makita, and C.-I. Meng (1991), A particle simulation of large-amplitude undulations on the evening diffuse auroral boundary, *J. Geophys. Res.*, *96*, 1439–1449.

Yamamoto, T., K. Makita, and C.-I. Meng (1993), A particle simulation of "giant" undulations on the evening diffuse auroral boundary, *J. Geophys. Res.*, *98*, 5785–5800.

Yamamoto, T., M. Ozaki, S. Inoue, K. Makita, and C.-I. Meng (1994), Convective generation of "giant" undulations on the evening diffuse auroral boundary, *J. Geophys. Res.*, *99*, 19,499–19,512.

Yamamoto, T., S. Inoue, N. Nishitani, M. Ozaki, and C.-I. Meng (1996), A theory for generation of the paired region 1 and region 2 field-aligned currents, *J. Geophys. Res.*, *101*, 27,199–27,222.

Yamamoto, T., S. Inoue, and C.-I. Meng (1997a), Formation of auroral omega bands in the paired region 1 and region 2 field-aligned current system, *J. Geophys. Res.*, *102*, 2531–2544.

Yamamoto, T., S. Inoue, and C.-I. Meng (1997b), Effect of anomalous cross-field diffusion on the field-aligned current generation, *J. Geomagn. Geoelectr.*, *49*, 923–945.

Yamamoto, T., S. Inoue, and M. Ozaki (1999), Latitudinal structure of the nightside region 1 field-aligned current observed from the EXOS-D satellite, *Adv. Polar Upper Atmos. Res.*, *13*, 105–118.

Yamamoto, T., M. Ozaki, and S. Inoue (2002), Evaluation of the region 1 field-aligned current from the low-latitude boundary layer using the 1989 Tsyganenko model, *Adv. Polar Upper Atmos. Res.*, *16*, 13–35.

Yang, Y. S., R. W. Spiro, and R. A. Wolf (1994), Generation of region 1 current by magnetospheric pressure gradients, *J. Geophys. Res.*, *99*, 223–234.

Zhang, Y., L. J. Paxton, D. Morrison, A. T. Y. Lui, H. Kil, B. Wolven, C.-I. Meng, and A. B. Christensen (2005), Undulations on the equatorward edge of the diffuse proton aurora: TIMED/GUVI observations, *J. Geophys. Res.*, *110*, A08211, doi:10.1029/2004JA010668.

T. Yamamoto, Department of Earth and Planetary Science, University of Tokyo, 3-1, Hongo 7 chome, Bunkyo-ku, Tokyo, 113-0033, Japan. (sty@mail.ecc.u-tokyo.ac.jp)